An Evaluation of Finite Element Models of Stiffened Plates

by

Ami Salomon

M.B.A, TECHNION – Israel Institute of Technology, 1999

B.Sc., Mechanical Engineering, TECHNION – Israel Institute of Technology, 1995

Submitted to the Department of Ocean Engineering

in Partial Fulfillment of the Requirements for the Degree of

Master of Science in Naval Architecture and Marine Engineering

at the

Massachusetts Institute of Technology

February 2001

Signature of Author .....
Department of Ocean Engineering
December 27, 2000

Certified by .....
Klaus-Jürgen Bathe
Professor of Mechanical Engineering
Thesis Supervisor

Certified by .....
David Burke
Senior Lecturer
Thesis Reader

Accepted by.....
Nicholas Patrikalakis
Kawasaki Professor of Engineering
Chairman, Department Committee on Graduate Studies

An Evaluation of Finite Element Models of Stiffened Plates

by

Ami Salomon

Submitted to the Department of Ocean Engineering

on December 27, 2000 in Partial Fulfillment of the

Requirements for the Degree of

Master of Science in Naval Architecture and Marine Engineering

Abstract

Several ways to model stiffened plate structures using the finite element method are discussed. Special attention is given to the assumptions involved within each finite element model. The modeling capabilities of the relevant elements are investigated thoroughly by constructing and solving finite element models of simple cantilever beam structures. In particular, the influence of the depth of the web on the performances of the different modeling methods is examined.

We evaluate three basic modeling methods, which differ by the way the stiffeners are modeled: two methods use beam elements (Hermitian and isoparametric beam elements) and the third uses shell elements. The displacement and stress solutions, obtained by these methods, are measured against solutions of a three-dimensional element model. We identify several limitations of the modeling methods under investigation, and we show that their performances are strongly depended on the depth of the stiffeners. We offer modifications to the different models, and we show them to be efficient for modeling stiffened plate structures with different boundary conditions. In particular, the modification of the classical and commonly used Hermitian beam elements is shown to yield excellent results.

Thesis Supervisor: Klaus-Jürgen Bathe
Title: Professor of Mechanical Engineering

Thesis Reader: David Burke
Title: Senior Lecturer

To my family

Acknowledgements

I would like to express my deep appreciation to my thesis supervisor, Professor Klaus-Jürgen Bathe, for his guidance and encouragement throughout my research work at M.I.T. He has shown great interest in my research, and his wise suggestions regarding my thesis work were always very helpful.

I am also very grateful to my thesis reader, Doctor David Burke, for his valuable remarks concerning my work and his encouragement during my studies at M.I.T. He has been both a teacher and a good friend to me.

I would also like to thank my colleagues in the Finite Element Research group at M.I.T for their continuous assistance. In particular, I would like to thank Sandra Rugonyi, Nagi El-Abbasi, Jean-François Hiller and Juan Pablo Pontaza for their valuable advises and friendship.

I would like to thank ADINA R&D, Inc for allowing me to use their proprietary finite element software ADINA for my research work. All the finite element results presented in this thesis were generated by this code.

I am also most thankful to the Israeli Navy and the Israeli ministry of defense for funding my studies at M.I.T and my staying in the United-States.

Last but not least, I would like to express my utmost gratitude to my parents and to my wife Yonit for their unconditionally love and support.

Table of contents

Abstract **2**

Acknowledgements **4**

Table of contents **3**

List of figures **7**

1 Introduction **9**

1.1 Background 9

1.2 Recent efforts in the field of static finite element analysis of stiffened plates 10

1.3 Thesis area of concentration. 12

2 Finite element formulation and assumption **15**

2.1 Physical problems, mathematical models, and finite element solution 15

2.2 General finite element formulation 17

2.2.1 Problem statement 17

2.2.2 The principle of virtual work 20

2.2.3 Finite element equations 21

2.3 Some aspects of the finite element formulation 24

2.3.1 Truss and beam elements versus general two- or three- dimensional elements. 24

2.3.2 Generalized coordinates finite elements versus iso-parametric finite elements. 25

3 Assumptions involved with relevant elements **30**

3.1 Beam elements 30

3.1.1 General beam considerations 30

3.1.2 Hermitian beam element 32

3.1.3 Iso-beam element 43

3.1.4 Comparison between Hermitian and iso-beam elements 46

3.2 Shell elements 47

4 A study of element modeling capabilities: analysis of cantilever beams 57
4.1 The purpose of this study 57
4.2 Finite elements models. 58
4.3 Summary of results 59
4.3.1 Three-dimensional model – the reference solution 60
4.3.2 Hermitian beam model 60
4.3.3 Iso beam model 66
4.3.4 All shell model 66
4.3.5 Over-all comparison 74
4.4 Conclusions reached from the analyses 75

5 Analyses of stiffened plate 77
5.1 Introduction 77
5.2 Analytical solution 79
5.3 Solutions of finite element models 82
5.3.1 Clamped edges boundary condition. 82
5.3.2 Simply-supported boundary conditions 91

6 Concluding remarks 96

References 99

Appendix A – Incompatibility of complex cross-sections 101

List of figures

2-1: The process of finite element analysis (taken from [2])....16
2-2: General three-dimensional body with an 8-node three-dimensional element....18
3-1: Beam deformation assumptions (taken from [2])....31
3-2: Hermitian beam element (taken from [16])....33
3-3: Axial forces F1 and F7....34
3-4: Twisting moments F4 and F10....36
3-5: Shear forces F2 and F8....37
3-6: Bending moments F6 and F12....41
3-7: Formulation of two-dimensional iso-beam element....45
3-8: Interpolation functions of two to four variable-number-nodes one-dimensional element (taken from [2])....45
3-9: Flat shell element - superposition of a plate element and a plan stress element....48
3-10: Deformation assumptions in analysis of plate including shear deformation....49
3-11: Interpolation functions of four to nine variable-number-nodes two-dimensional element (taken from [2])....52
3-12: Four node two-dimensional element....54
4-1: Cross-sections of cantilever beams under investigation....58
4-2: Finite element models of cantilever beam with a "T" cross-section....59
4-3: Bending deflection of beam with "T" cross-section, comparison of 3D model solution to analytical beam theory solution....61
4-4: Deflection of a "T" beam – original and modified Hermitian beam models....61
4-5: Original and modified Hermitian beam models – definition of cross-section....63
4-6: Bending stresses in "T" cross-section beam....65
4-7: Shear stress due to bending in a web of a "T" cross-section beam....65
4-8: "All-shell" models of a beam with "T" cross-section....67
4-9: Cantilever beam with "T" cross-section – evaluation of the "all-shell" models tip displacement solution....68

4-10: Cantilever beam with wide flange "T" cross-section – evaluation of the "all-shell" models tip displacement solution 70
4-11: Modified "all-shell" model – definition of cross-section 71
4-12: Modified web depth and moment of inertia. 73
4-13: "All-shell" model – bending stresses 74
4-14: Cantilever "T" beam – comparison of all models to the 3D model 75
5-1: Geometry of the stiffened plate under investigation. 78
5-2: Finite element models of stiffened plate. 78
5-3: Definitions of the terms in the Huber equation. 81
5-4: Solution of the Huber equation. 82
5-5: Stiffened plate with clamped edges – maximum displacement as function of the depth of the stiffeners. 84
5-6: Discrepancy of the maximum displacement as predicted by the various models relative to the three-dimensional model solution 84
5-7: Intersection between plate and stiffener 86
5-8: Shear lag in a wide flange "T" beam. 88
5-9: Stiffened plate with clamped edges – bending stresses in the stiffeners 90
5-10: Stiffened plate with clamped edges – evaluation of bending stresses. 90
5-11: Stiffened plate with simply supported edges – maximum displacement as function of the depth of the stiffeners. 93
5-12: Stiffened plate with simply supported edges – discrepancy of displacement solutions from the 3D model solution 93
5-13: Stiffened plate with simply supported edges – bending stresses in the stiffeners 95
5-14: Stiffened plate with simply supported edges – discrepancy of bending stresses solutions from the 3D model solutio 95
A-1: "T" cross-section modeled by Hermitian beam elements 102
A-2: Geometrical constrains and incompatibility of the displacements of the eccentric beam. 106
A-3: Cantilever beam modeled with 2n elements – n in the flange, n in the web. 107
A-4: Comparison of tip deflection solution. 108

1 Introduction

1.1 Background

A stiffened plate structure is a common occurrence. Its application exists in various engineering structures; namely, ship hulls, offshore structures, rail/road bridges, aircraft structures, printed circuits boards and many others. In a stiffened plate, stiffeners may occupy any position depending on the design requirements. The objective is to make an efficient structural arrangement to sustain the externally applied forces with minimum material weight, by limiting the displacements and stresses to their permissible values. These stiffened plate structures are highly indeterminate in nature and as such they pose a great challenge to the analysts.

The different approaches available for the analysis of stiffened plate problems can be put under three broad categories: orthotropic plate model, grillages and plate-beam systems.

Huber [9] considered the orthotropic plate model in which the stiffened plate is replaced by a bare plate with orthotropic properties. This model, which is often referred to as the smearing technique model, is used efficiently if the stiffeners are small, identical and placed uniformly at close intervals. Identical stiffener profiles and equal spacing of stiffeners impose limitations on the use of this model and further, the evaluation of the stresses in the plate and in the stiffeners creates additional difficulties.

Idealization of a stiffened plate as a grillage starts with the assumption of an effective breadth of plating. According to various researches this effective breadth varies from 50% to 80% of the stiffener spacing. The comparatively complicated theories for plated grillages, as put forward by Kendrick [11] and Clarkson [5] have indicated that good results may be obtained for design work by a grillage calculation. This method of analysis gives deflections normally within 5% and occasionally within 10%, and the beam stresses vary generally within 10% to 20% of the experimental values.

The analysis of a stiffened plate structure as a plate-beam system, which reflects the true or near-true nature of the physical problem behavior, was enabled with the advent of digital computers, which resulted in attempts to solve the problem with numerical methods. Among the numerical methods, the finite element method is the most powerful one, and indeed great research effort was made in trying to achieve accurate and efficient finite element models for stiffened plates.

1.2 Recent efforts in the field of static finite element analysis of stiffened plates

The field of static finite element analysis of stiffened plates was studied extensively and much literature can be found on the subject. The following is a brief summary of some of the significant studies conducted in the recent years.

Cho and Vorus [4] proposed a three-dimensional method for analyzing stiffened plate structures. Their work was based on a formerly derived well-known method that uses two dimensional plane-stress elements and one-dimensional beam elements. The connection between the stiffeners and the plate is incorporated through constraints imposed on the relationship of rotational and translation displacements between the two element systems. In this model the displacement compatibilities of the beam and plate elements is satisfied only at the nodal points. The contacting shear compatibility condition along the elements is not maintained.

The contribution of the authors was the modification of this model to allow for continuous shear transmission between the plate and the matching beam elements along the joining lines. This is done by imposing equal strain along the interface of the plate and the stiffeners, which leads to correction terms in the global stiffness matrix. The derivation of the correction terms is based on a simple case in which a complex beam is modeled by two beam elements, and hence the incorporation of the method to a stiffened plate structure requires the knowledge of the effective breadth of the plate, which is difficult to obtain accurately. The paper concludes with numerical examples in which a

good performance of the modified method is reported.

Mukhopadhyay and Satsangi [13] developed isoparametric *stiffened plate elements* for the analysis of stiffened plate structures. The concept of a stiffened plate element is based on the projection of the stiffener stiffness to the nodes of the plate element. This approach enables flexibility in the analysis process, since the location of the stiffeners can be redefined, without changing the plate element mesh. The evaluation of the element matrices is based on the following assumptions: (i) the bending deformations follow Mindlin's hypothesis which allow shear deformation; therefore straight planes which are perpendicular to the mid-surface of the plate, remain straight but not normal to the deformed mid-surface; (ii) the deflection w in the z-direction is a function of x and y only; (iii) the stresses in the z-direction are assumed to be zero irrespective of the loading (plane stress condition); and (iv) the displacements of the points on the mid-surface in the normal direction to this plane is small in comparison to the thickness of the plane.

The authors have shown that the element is capable of idealizing structures such as concentrically and eccentrically stiffened plates, but it is limited to modeling of orthogonal stiffened plates.

O'Leary and Harari [14] developed a stiffened plate finite element from a constraint variational principle, using Lagrange multipliers to impose the constraints between the stiffeners and the plate. In the development of the stiffened plate element, the bending and membrane behaviors are treated separately. The stiffness matrix of the plate was augmented by formulating the beam element stiffness with additional terms to impose the constraints between the stiffener and the plate. Even though the shear distortion is not included in the element formulation, the method was shown to be efficient and reliable in modeling thin flat plates reinforced with relatively widely spaced, heavy stiffeners.

Boot and Moore [3] attempted to identify the generalized conditions under which stiffened plates can be approximated as a two-dimensional orthotropic plate. This approximation is based on the concept of smoothed flexural, torsional and transverse shear rigidities. The authors obtained, by making suitable assumptions, a simplified set of

constitutive equations defining the stiffened plate problem, subjected to elastic behavior. The significance of these assumptions is investigated under a wide range of conditions, and the results calculated for typical problems using the simplified theory are compared with experimentally obtained data. The authors concluded that a two-dimensional approximation can be theoretically justified only if the stiffeners form an *orthogonal* network. They also concluded that the assumption of centroidal neutral axes is sufficiently accurate under arbitrary conditions for engineering purposes. However, the stresses generated in the stiffeners due to Poisson's ratio effects, which are normally ignored, may be significant.

1.3 Thesis area of concentration.

As described above, a wide range of element types has been proposed for the analyses of stiffened plates. However, we can identify three basic types of finite element *models* that are widely used by analysts, and are available in most of the finite element codes. These model types can be summarized as: I) orthotropic plate model, II) plate-beam systems and III) models in which the stiffeners, as well as the plate, are built up from plate/shell elements. This thesis work concentrated on the evaluation of model types II) and III), compared with a full three-dimensional model.

The accuracy of solution of a physical problem model depends on the information contained in the mathematical (and therefore finite element) model that describes the physical problem. Since a real structure is obviously three-dimensional, only three-dimensional elements can model the real physical problem without undertaking assumptions concerning the mechanics of the structure. The assumptions involved with the one- and two- dimensional elements lead to simpler and cheaper (in computer resources and engineering time) models, but also to lack of ability to predict some physical phenomena.

The goal of this research is to conclude whether certain simplified finite element

models can provide satisfactory engineering results despite the assumptions involved in them.

In the category of the plate-beam systems, two different types of models were investigated; in each type different beam elements and constraints between the beams and the plate were used. In both cases, the plate was modeled with flat *shell* elements.

In the first plate and beam element model, *Hermitian beam* elements are used. These two-noded elements are formulated by solving the beam differential equations of equilibrium and hence yield the *exact* (within beam theory) solution of simple beam structures, even when a very coarse mesh is used (see detailed description of the element formulation in Section 3.1.2). The Hermitian beams are placed along the nodal lines of the shell elements, in the plane of the plate. The eccentric position of the stiffeners in the real structure is modeled by assigning an offset value to the beam elements, which results in constraints between the beam and the shell degrees of freedom.

In the second plate and beam element model, isoparametric beam elements are used. These elements are formulated using the virtual work principle, and the differential equilibrium equations are not satisfied exactly. As a result, the solution of the mathematical model (see Section 2.1) is approached only when a relatively large number of elements is used. The isoparametric beam elements (which are referred to as "iso-beam" elements below) can have one or two internal nodes along the element, and hence better (relative to the Hermitian beam elements) compatibility can be obtained with shell elements that have internal nodes along the edges.

The iso-beam elements are constrained to the plate by rigid links: the nodal displacements of the beam element are made to undergo the displacements prescribed by the corresponding nodes of the shell element.

The second general type of models that was investigated (marked as model type III above) is the "all-shell" model, in which the stiffeners (as well as the plate) are built up from shell elements. This type of models is obviously more expensive in computer resources and engineering time than models which use beam elements to model the stiffeners, but they are a better representation of the real physical problem.

The performances of the models described above were compared with a three-dimensional model. The use of a three-dimensional model is extremely expensive (about one order of magnitude more expensive in computer resources than a two-dimensional model), and hence it is rarely used to model stiffened plates. As mentioned above, the formulation of a general three-dimensional element is free from a priori kinematic structural assumptions about the material particle behavior (of course, the finite element displacement assumptions are present) and hence an assembly of three-dimensional elements can be an excellent replica of nature, provided that the mesh of the elements is fine enough. For this reason, three-dimensional models were constructed and solved for each variation of the stiffened plate structure that was analyzed by the simplified finite element models, in order to obtain a "reference solution" with which the solutions could be compared.

In order to gain insight into the modeling capabilities of the different elements, some simple geometries of cantilever beams (with various cross-sections) were examined. The cantilever beams were modeled using the same modeling methods as in the case of the stiffened plate analysis (see detailed description in Chapter 4). The study using the beam geometries led to several conclusions that proved to be valuable for the analysis of a stiffened plate structure.

The performances of the models were investigated with different stiffener depths. It was found that the accuracy of the various modeling methods is strongly dependent on the depth of the stiffeners.

2 Finite element formulation and assumption

2.1 Physical problems, mathematical models, and finite element solution

Figure 2-1 (taken from [2]) summarizes the finite element solution process. This process is usually used to solve physical problems such as structures subjected to certain loads. We use assumptions to idealize the physical problem as a mathematical model, which is stated by a set of differential equations, and we use the finite element procedure to solve the mathematical model.

It is important to note that only the selected mathematical model is solved by the finite element method, and hence the accuracy with which the physical problem is modeled is totally governed by the mathematical model that we choose to use. Even the most refined mesh cannot contain all the information that exists in the real physical problem, and hence the solution of the mathematical model can only give us an approximation of the real response.

We choose the mathematical model according to the phenomena we want to predict (small deflections, nonlinear response, etc.), and we must make sure that we choose reliable and effective models. A reliable model is one that predicts the required response within a selected level of accuracy. An effective model is one that yields the required response at relatively low cost.

The reliability and effectiveness of a given model can be examined versus a solution of a more comprehensive model of the same physical problem. In general, the most comprehensive model that can be thought of is a three-dimensional model that also includes nonlinear effects. Therefore, it may be necessary to solve higher-order mathematical models in order to asses the solution of the chosen model.

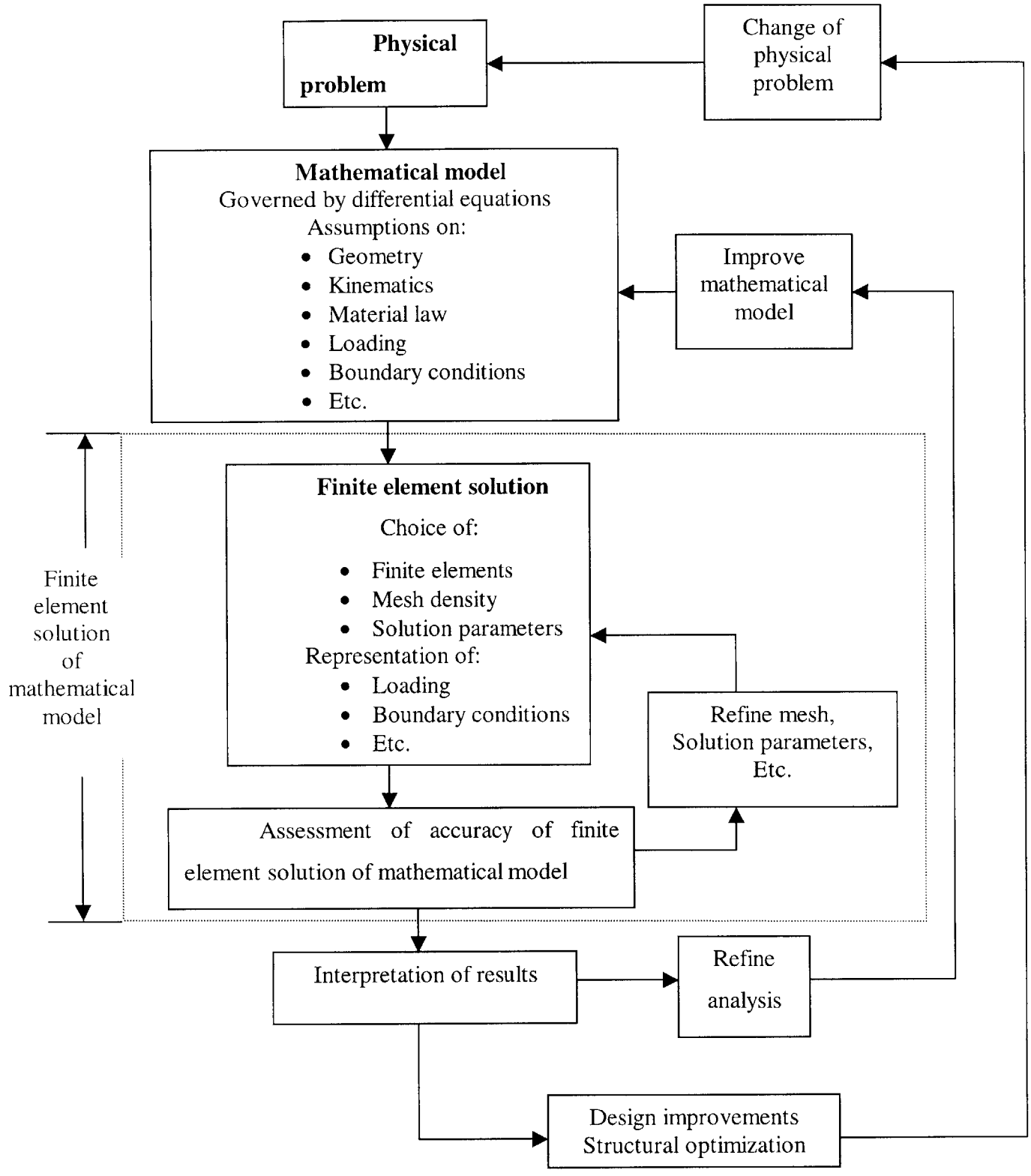

Figure 2-1: The process of finite element analysis (taken from [2]).

As discussed in details in the following chapters, a beam structure can be analyzed by a sequence of such mathematical models. The beam may first be analyzed using Bernoulli beam theory, then Timoshenko beam theory, then two-dimensional plane stress theory, and finally using a full three-dimensional continuum. Such a sequence of models is referred to as a hierarchy of models. It is obvious that a model higher in the hierarchy yields to a more accurate prediction of nature, but it is also more expensive in computer resources and engineering time. In most common cases, a full three-dimensional analysis is about an order of magnitude more expensive than a two-dimensional solution.

We can summarize the basic steps in the process of analysis using finite elements as the proper choice of the mathematical model, the solution of the model by finite element procedures and the evaluation of the results. We must judge, for each finite element analysis, if an appropriate mathematical model was chosen (in light of the characteristics of the physical problem) and if the model was solved to sufficient accuracy.

2.2 General finite element formulation

In this section we begin by stating the general elasticity problem to be solved. We then discuss the principle of virtual displacements, which is the basis of the finite element solution, and we describe the derivations of the finite element equations. It should be mentioned that in the following we use the approach given in [2].

2.2.1 Problem statement

Figure 2-2 (taken from [2]) shows a general three-dimensional body that will serve to demonstrate the general problem to be solved. The body is supported on the area S_u with prescribed displacements U^{S_U} and is subjected to surface loads (force per unit area) f^{S_f} on the surface area S_f.

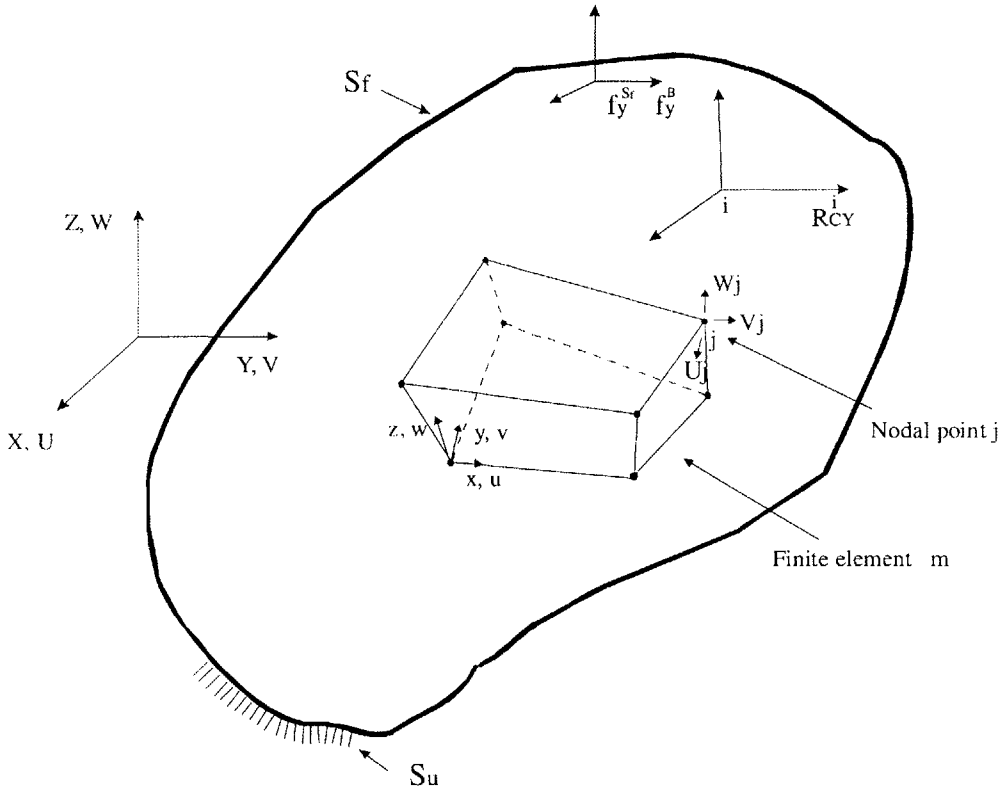

Figure 2-2: General three-dimensional body with an 8-node three-dimensional element.

The body is also subjected to body forces f^B (per unit volume) and concentrated loads R_C^i (i indicates the point where the load is applied). The externally applied forces have three components corresponding to the X,Y,Z coordinate axes:

$$f^B = \begin{bmatrix} f_x^B \\ f_y^B \\ f_z^B \end{bmatrix}; \quad f^{S_f} = \begin{bmatrix} f_x^{S_f} \\ f_y^{S_f} \\ f_z^{S_f} \end{bmatrix}; \quad R_C^i = \begin{bmatrix} R_{Cx}^i \\ R_{Cy}^i \\ R_{Cz}^i \end{bmatrix} \tag{2.1}$$

The displacements of the body are denoted as:

$$U(X,Y,Z)=\begin{bmatrix} U \\ V \\ W \end{bmatrix} \tag{2.2}$$

where on the surface area S_u we demand $U = U^{S_U}$. The strains corresponding to the displacements above are:

$$\varepsilon^T = [\varepsilon_{xx}\ \ \varepsilon_{yy}\ \ \varepsilon_{zz}\ \ \gamma_{xy}\ \ \gamma_{yz}\ \ \gamma_{zx}] \tag{2.3}$$

where:

$$\varepsilon_{xx} = \frac{\partial U}{\partial X};\quad \varepsilon_{yy} = \frac{\partial V}{\partial Y};\quad \varepsilon_{zz} = \frac{\partial W}{\partial Z}$$

$$\gamma_{xy} = \frac{\partial U}{\partial Y} + \frac{\partial V}{\partial X};\quad \gamma_{yz} = \frac{\partial V}{\partial Z} + \frac{\partial W}{\partial Y};\quad \gamma_{zx} = \frac{\partial W}{\partial X} + \frac{\partial U}{\partial Z} \tag{2.4}$$

The stresses which corresponds to the strains are:

$$\tau^T = [\tau_{xx}\ \ \tau_{yy}\ \ \tau_{zz}\ \ \tau_{xy}\ \ \tau_{yz}\ \ \tau_{zx}] \tag{2.5}$$

where

$$\tau = C\varepsilon + \tau^I \tag{2.6}$$

In (2.6) C is the stress-strain material matrix and the vector τ^I indicates initial stresses.

The problem to be solved is now defined by the geometry of the body, the applied loads, the boundary condition, the material law and the initial stresses. Our objective is to obtain the displacement field, and by doing so to derive the strains and stresses.

In the following we assume linear analysis conditions, which require that the displacements are infinitesimally small. A consequence is that we can express the equilibrium of the body with respect to its unloaded configuration with the calculation of the strains by (2.4). We also require that the relation between the strains and stresses is constant (not dependent on the loading or stresses), although it might vary inside the body.

2.2.2 The principle of virtual work

The principle of virtual work (also known as the principle of virtual displacements) is the basis of the displacement-based finite element procedures. It states that the equilibrium of any general body requires that for any field of virtual displacements that the body virtually undergoes, the total internal virtual work is equal to the total external virtual work. This can be stated as

$$\int_V \bar{\varepsilon}^T \tau \, dV = \int_V \bar{U}^T f^B dV + \int_{S_f} \overline{U^{S_f}}^T f^{S_f} dS + \sum_i \bar{U}^{iT} R_C^i \tag{2.7}$$

where $\bar{U}$ is the virtual displacement field and $\bar{\varepsilon}$ indicates the virtual strains.

It is important to note that the body does not physically undergoes the virtual displacement field $\bar{U}$, since this displacement field is totally independent of the actual loading. The virtual displacements are only used to invoke the equilibrium of the body, as stated above.

When the principle of virtual work is fulfilled for all allowable virtual displacement fields, the three fundamental requirements of mechanics – namely, differential equilibrium, compatibility and the stress-strain law are satisfied.

2.2.3 Finite element equations

The essence of the finite element analysis is the approximation of the body as an assemblage of finite elements, which are connected through the nodes at their boundaries. In each element, the displacements are assumed to be a function of the displacements at the nodes. Hence, for a given element m, we can write:

$$u^{(m)}(x, y, z) = H^{(m)}(x, y, z)\, \hat{U} \tag{2.8}$$

where $H^{(m)}$ is the displacement interpolation matrix, and $\hat{U}$ denotes the displacements at all nodal points, including those at the supports of the body. $\hat{U}$ is a vector of dimension 3N, where N is the number of the nodes of the element assemblage:

$$\hat{U}^T = [U_1\ V_1\ W_1 \quad U_2\ V_2\ W_2\ \ldots\ U_N\ V_N\ W_N] \tag{2.9}$$

A typical finite element is shown in figure 2-2. The mesh of the complete body corresponds to the assemblage of all elements (or elements with different geometry) such that no gaps are left.

It is important to note that the displacement field (and hence strains) within a given element is influenced only by the displacements of the nodes of this element.

The strains that correspond to the displacement vector $\hat{U}$ are:

$$\varepsilon^{(m)}(x, y, z) = B^{(m)}(x, y, z)\hat{U} \tag{2.10}$$

where $B^{(m)}$ is the strain-displacement matrix, constructed by using the relations in (2.4). The stress vector can be stated as:

$$\tau^{(m)} = C^{(m)}\varepsilon^{(m)} + \tau^{I(m)} \tag{2.11}$$

where $C^{(m)}$ is the stress-strain matrix of element m and $\tau^{I(m)}$ denotes the initial stresses. The material law (which is specified in $C^{(m)}$) can vary within the element assemblage.

We can now derive the equilibrium equations that correspond to the finite element assemblage, by rewriting (2.7) as a sum of integration over the volume and areas of all finite elements:

$$\sum_m \int_{V^{(m)}} \bar{\varepsilon}^{(m)^T} \tau^{(m)} dV^{(m)} = \sum_m \int_{V^{(m)}} \bar{u}^{(m)^T} f^{B(m)} dV^{(m)} + \sum_m \int_{S_1^{(m)} \ldots S_q^{(m)}} \bar{u}^{s(m)^T} f^{s(m)} dS^{(m)} + \sum_i \bar{u}_i^T R_c^i \tag{2.12}$$

where m=1,2,...,k , k being the number of elements, and $S_1^{(m)},...,S_q^{(m)}$ denotes the element surfaces that are part of the body surface S.

We use the relations in (2.8) and (2.10) to obtain the virtual displacements and strains:

$$\bar{u}^{(m)}(x, y, z) = H^{(m)}(x, y, z)\, \bar{\hat{U}} \tag{2.13}$$

$$\bar{\varepsilon}^{(m)}(x, y, z) = B^{(m)}(x, y, z)\bar{\hat{U}} \tag{2.14}$$

By substituting into (2.12), we get:

$$\bar{\hat{U}}^T [\sum_m B^{(m)T} C^{(m)} B^{(m)} dV^{(m)}]\hat{U} = \bar{\hat{U}}^T [\{\sum_m \int_{V^{(m)}} H^{(m)T} f^{B(m)} dV^{(m)}\} +$$

$$+\{\sum_m \int_{S_1^{(m)} \ldots S_q^{(m)}} H^{s(m)T} f^{S(m)} dS^{(m)}\} - \{\sum_m \int_{V^{(m)}} B^{(m)T} \tau^{I(m)} dV^{(m)}\} + R_C] \tag{2.15}$$

We can take $\hat{U}$ and $\bar{\hat{U}}$ out of the summation signs since they are independent of any particular element. In order to obtain the equations for the unknown nodal point

displacements, we use the principle of virtual work n times by imposing unit virtual displacements for all components of $\overline{\hat{U}}$. The result is:

$$K\hat{U} = R \tag{2.16}$$

The matrix K is the stiffness matrix of the element assemblage,

$$K = \sum_{m} \int_{V^{(m)}} B^{(m)T} C^{(m)} B^{(m)} dV^{(m)} \tag{2.17}$$

The load vector R is given by:

$$R = R_B + R_S - R_I + R_C \tag{2.18}$$

where R_B is the effect of the element body forces,

$$R_B = \sum_{m} \int_{V^{(m)}} H^{(m)T} f^{B(m)} dV^{(m)} \tag{2.19}$$

R_S is the effect of the element surface forces,

$$R_S = \sum_{m} \int_{S_1(m),\ldots,S_q(m)} H^{S(m)T} f^{S(m)} dS^{(m)} \tag{2.20}$$

R_I is the effect of the element initial stresses,

$$R_I = \sum_{m} \int_{V^{(m)}} B^{(m)T} \tau^{I(m)} dV^{(m)} \tag{2.21}$$

and R_C is the vector of the nodal concentrated loads.

2.3 Some aspects of the finite element formulation

In the following we discuss some aspects concerning finite element formulations and we distinguish between several groups within the family of finite elements. In Chapter 3, where we describe the formulation of the elements that were used along the course of this research, we revisit these formulation aspects.

2.3.1 Truss and beam elements versus general two- or three- dimensional elements.

• Truss and beam elements.

Originally, the truss and beam element assemblages were not referred to as finite element models since the exact (within beam theory) stiffness matrices of these elements can be calculated by solving the differential equations of equilibrium of the elements rather than by using the principle of virtual work. As a result, all three requirements of an exact solution (the stress equilibrium, the compatibility, and the constitutive requirements) are fulfilled, and hence the *exact* element internal displacement and stiffness are calculated.

• General two- and three- dimensional finite elements.

We use the principle of virtual work to formulate the stiffness matrix of two- and three- dimensional finite elements. Since we do not know the exact displacement variation (as in the case of a beam element) we use various functions that approximate the actual displacements. As a result, the differential equations of equilibrium are not satisfied, but this error vanishes as we refine the mesh.

2.3.2 Generalized coordinates finite elements versus iso-parametric finite elements.

In the discussion below we distinguish between two methods that serve to assemble the finite elements matrices: generalized coordinates and iso-parametric formulations. The first method enhance the understanding of the finite element method, while the other is more effective in most practical analyses. It should be mentioned that in the discussion below we use the finite element matrices derivations given in [2].

• Generalized coordinates finite elements

The derivation of the generalized coordinate finite elements is based on the approximation of the element displacements as polynomials in x,y and z with undetermined constant coefficients α_i, β_i and γ_i, i=1,2,..., referred to as *generalized coordinates*.

In the general case we have:

$$\begin{aligned} u(x,y,z) &= \alpha_1 + \alpha_2 x + \alpha_3 y + \alpha_4 z + \alpha_5 xy + \ldots \\ v(x,y,z) &= \beta_1 + \beta_2 x + \beta_3 y + \beta_4 z + \beta_5 xy + \ldots \\ w(x,y,z) &= \gamma_1 + \gamma_2 x + \gamma_3 y + \gamma_4 z + \gamma_5 xy + \ldots \end{aligned} \tag{2.22}$$

where α_i, β_i and γ_i are the generalized coordinates. The relation in (2.22) can be written in matrix form,

$$u = \Phi\alpha \tag{2.23}$$

where Φ contains the polynomials terms, and α is a vector of the generalized coordinates. In order to state the generalized coordinates as functions of the nodal point displacements, we evaluate the relation in (2.23) for $\hat{u}$ (which denotes the displacements at the nodes):

$$\hat{u} = A \cdot \alpha \tag{2.24}$$

If A is not singular, we get:

$$\alpha = A^{-1} \cdot \hat{u} \tag{2.25}$$

The generalized strain vector is given by:

$$\varepsilon = E\alpha \tag{2.26}$$

where the terms in the matrix E are obtained by using the displacement approximation given in (2.22). The stresses τ are obtained by:

$$\tau = CE \tag{2.27}$$

From (2.23) to (2.27), we obtained all the terms needed for the evaluation of the finite element matrices. Using the notation of Section 2.2, we have:

$$H = \Phi A^{-1} \tag{2.28}$$

$$B = EA^{-1} \tag{2.29}$$

• Iso-parametric elements.

The essence of the iso-parametric finite element formulation is the direct relationship between the element displacements at any point in the element and the element nodal point displacements, which is established through the use of interpolation functions. As a result, there is no need to calculate the transformation matrix A^{-1} [see (2.25)]; Instead, the element matrices are obtained directly.

The element coordinates and displacements are expressed in the form of an interpolation using the natural coordinate system of the element. This coordinate system may be one-, two-, or three dimensional, depending on the dimensionality of the element. Considering a general three-dimensional element, the coordinate interpolations are:

$$x = \sum_{i=1}^{q} h_i x_i ; \qquad y = \sum_{i=1}^{q} h_i y_i ; \qquad z = \sum_{i=1}^{q} h_i z_i \tag{2.30}$$

where x, y and z are the coordinates at any point in the element, and x_i, y_i, z_i, i=1,...,q , are the coordinates of the q element nodes. The interpolation functions h_i are defined with the variables of the natural coordinate system of the element. These variables – r, s and t – vary from –1 to +1. We use only the r variable in the case of the one-dimensional element, r and s for two-dimensional elements and r,s,t for a three-dimensional case. The principal property of a certain interpolation function, say h_i, is that its value is unity at node i and zero at all the other nodes of the element. This fundamental property enables a systematic derivation of the interpolation functions.

The element displacements are interpolated using the same method:

$$u = \sum_{i=1}^{q} h_i u_i ; \qquad v = \sum_{i=1}^{q} h_i v_i ; \qquad w = \sum_{i=1}^{q} h_i w_i \tag{2.31}$$

where u, v, and w are the displacements at any point in the element and u_i, v_i and w_i, are the displacements at the nodes.

In order to evaluate the element stiffness matrix, we have to calculate the strain displacement transformation matrix. We obtain the element strains via derivatives of the element displacements with respect to the local coordinates. Since these displacements include natural coordinate variables, we need to relate the x,y,z derivatives to the r,s,t derivatives. We can rewrite (2.30) as:

$$x = f_1(r,s,t); \quad y = f_2(r,s,t); \quad z = f_3(r,s,t) \tag{2.32}$$

where the f_i imply that x, y and z are functions of the natural coordinate variables. We obtain the required derivatives, $\partial/\partial x$, $\partial/\partial y$ and $\partial/\partial z$ by using the chain rule:

$$\begin{bmatrix} \partial/\partial r \\ \partial/\partial s \\ \partial/\partial t \end{bmatrix} = \begin{bmatrix} \partial x/\partial r & \partial y/\partial r & \partial z/\partial r \\ \partial x/\partial s & \partial y/\partial s & \partial z/\partial s \\ \partial x/\partial t & \partial y/\partial t & \partial z/\partial t \end{bmatrix} \begin{bmatrix} \partial/\partial x \\ \partial/\partial y \\ \partial/\partial z \end{bmatrix} \tag{2.33}$$

or in a short matrix form,

$$\frac{\partial}{\partial r} = J \frac{\partial}{\partial x} \tag{2.34}$$

where J is the Jacobian operator. Since we need the derivatives with respect to the local coordinates, we use:

$$\frac{\partial}{\partial x} = J^{-1} \frac{\partial}{\partial r} \tag{2.35}$$

The inverse of J exists if there is a unique relation between the natural and the local coordinates of the element, as expressed in (2.32). Using (2.31) and (2.35), we evaluate the derivatives of the displacements, and construct the strain-displacement transformation matrix B, with

$$\varepsilon = B\hat{u} \tag{2.36}$$

where $\hat{u}$ denotes the element nodal point displacements. The element stiffness matrix is then given by

$$K = \int_V B^T C\, B\, dV \tag{2.37}$$

Since the terms in B are functions of the natural coordinates, the volume integration is conducted over the natural coordinate volume. Hence, the volume differential dV must also be written in terms of the natural coordinates:

$$dV = \det(J)\, dr\, ds\, dt \tag{2.38}$$

where det (J) is the determinant of the Jacobian operator in (2.34).

3 Assumptions involved with relevant elements

The understanding of the mechanical assumptions involved in each finite element used in a finite element analysis is essential for an educated judgment of the results obtained by the finite element solution. In this chapter, we discuss the assumptions involved with the elements that were used along the course of the research work.

As briefly described in Section 1.3, three types of elements were used during the thesis work: beam elements (including two sub-types: Hermitian beams and isoparametric beams), shell elements and three-dimensional elements. In the following we discuss the assumptions involved with the beam and the shell elements, and we present brief descriptions of the element formulations. It should be noted that there are no structural assumptions involved with the three-dimensional elements, a fact that enables excellent modeling capabilities but also leads to high cost in computer resources and engineering time.

3.1 Beam elements

We begin the beam elements description with a discussion of general beam considerations. These considerations relate to both beam element types (Hermitian and isoparametric [or in short "iso"] beam elements) that are presented afterwards.

3.1.1 General beam considerations

The classic bending analysis does not account for shear deformation. As a result, a normal to the neutral axis of the beam stays straight during and after deformation, and its rotation is equal to the rotation of the beam neutral axis. This hypothesis, which relates to the Bernoulli beam theory, is illustrated in Figure 3-1a (taken from [2]). The above

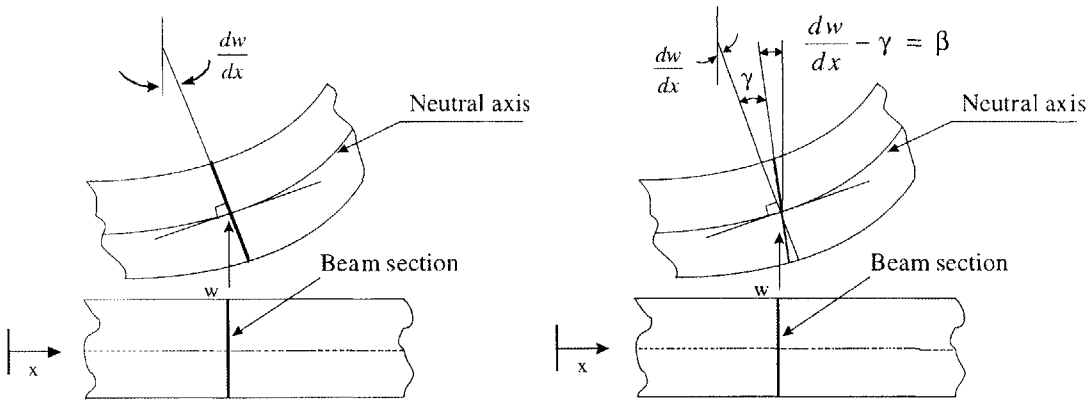

3-1a
Beam deformation
excluding shear effect

3-1b
Beam deformation
including shear effect

Figure 3-1: Beam deformation assumptions (taken from [2]).

assumption results into the well-known differential equation in which the transverse displacement w is the only variable.

The inclusion of shear deformations corresponds to Timoshenko's beam-bending theory. According to this theory, a normal to the neutral axis stays straight, but due to shear deformation it does not remain perpendicular to the neutral axis. As shown in Figure 3-1b, the total rotation of such a fiber is the difference between the rotation of the tangent to the neutral axis and the shear deformation,

$$\beta = \frac{dw}{dx} - \gamma \tag{3.1}$$

where γ is the shear strain across the section. The actual shear strain varies across the section, and hence the shear strain γ in (3.1) is an equivalent constant strain over a corresponding shear area A_s,

$$\tau = \frac{V}{A_s}; \quad \gamma = \frac{\tau}{G}; \quad A_S = k\,A \tag{3.2}$$

where V is the shear force at the section. Various hypotheses may be used in order to evaluate the shear correction factor, k (see [18] for details). One possibility is to assume that when acting on A_s, the *equivalent* shear stress must result in the same shear strain energy as the *actual* shear stress acting on the real cross-sectional area A. As shown in [18], this procedure leads to k=5/6 for a rectangular cross-section.

3.1.2 Hermitian beam element

3.1.2.1 General description

The Hermitian beam element is formulated by solving the beam differential equations of equilibrium (see discussion in Section 2.3.1). As a result, all three requirements of exact solution – namely, the stress equilibrium, the compatibility, and the constitutive requirements are fulfilled, and the exact ("exact" within beam theory) element stiffness and displacements are obtained.

The Hermitian beam is a 2-node element with a constant cross-section and 6 degrees of freedom at each node (see Figure 3-2). The displacements modeled by the beam element are cubic transverse displacements, linear longitudinal displacement and linear torsional displacement. Off-centered beams can be modeled by using an offset definition.

3.1.2.2 Formulation of Hermitian beam element.

In the following we describe the formulation of the Hermitian beam element using the approach presented in [16]. We describe the formulation for an element representing a straight beam with uniform cross-section, which can carry axial forces, bending moments and twisting moments. The various forces and moments acting on the beam are the axial forces F_1 and F_7; shearing forces F_2, F_3, F_8 and F_9; bending moments F_5, F_6, F_{11} and F_{12}; and twisting moments (torques) F_4 and F_{10}. The location and positive directions of these

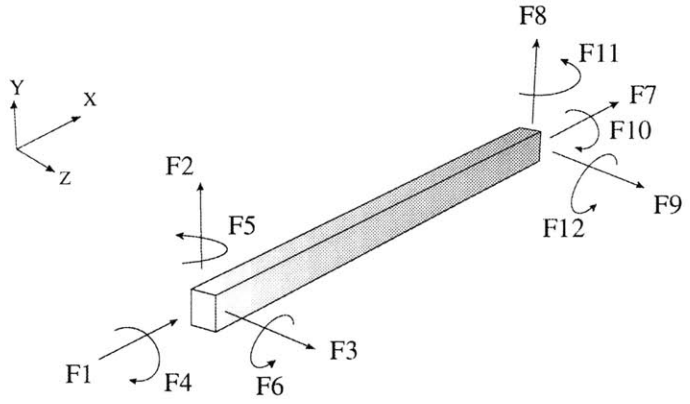

Figure 3-2: Hermitian beam element (taken from [16]).

forces are shown in Figure 3-2. The corresponding displacements $u_1,\ldots,u_{12}$ are taken to be positive in the positive directions of the forces.

In the following we assume that the axial forces act along the centroidal axis of the beam, and that the shearing forces and the bending moments act in the planes of the principal axes of the beam's cross-section. Consequently, the shearing forces and the bending moments that act in the x-y plane (F_2 ,F_8, F_6 and F_{12}) yield displacement that are decoupled from the shearing forces and bending moments in the x-z plane (F_3, F_{10}, F_5 and F_{11}). As a result, all forces (F_1 to F_{12}) can be divided into six groups, which can be treated independently of each other. Considering each group separately, we derive the corresponding stiffness terms, which together assemble the element stiffness matrix – as described below.

- Axial forces (F_1 and F_7)

The axial displacement shown in Figure 3-3 is obtained from the equation

$$F_1 = -\frac{du}{dx}EA \tag{3.3}$$

The integration of Equation (3.3) gives

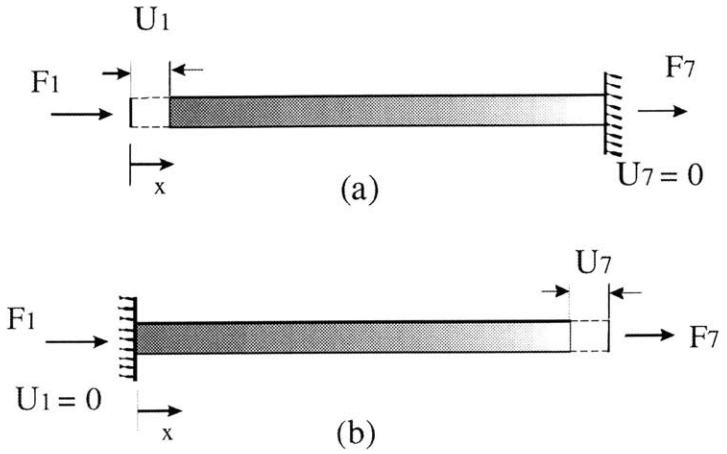

Figure 3-3: Axial forces F1 and F7.

$$F_1 x = -uEA + C_1 \tag{3.4}$$

where C_1 is a constant of integration. Imposing displacement u_1 at x=0, and zero displacement at x=l yields

$$C_1 = F_1 l \tag{3.5}$$

Using equations (3.4) and (3.5), for x=0 we get

$$F_1 = \frac{EA}{l} u_1 \tag{3.6}$$

From equilibrium in the x direction we have

$$F_1 = -F_7 \tag{3.7}$$

We use the force-displacement relation, F=ku, to define the individual stiffness terms k_{ij}. The physical meaning of the term k_{ij} is the element force F_i due to unit displacement u_j. Therefore

$$k_{11} = \left(\frac{F_1}{u_1} \right) = \frac{EA}{l} \tag{3.8}$$

and

$$k_{71} = \left(\frac{F_7}{u_1} \right) = -\frac{EA}{l} \tag{3.9}$$

Since the axial displacement is uncoupled from the other displacements, the rest of the terms in the first column of the stiffness matrix are equal to zero. Similarly, if $u_1=0$ and u_7 is nonzero (as demonstrated in Figure 3-3b), we have

$$k_{77} = \frac{EA}{l} \tag{3.10}$$

• Twisting moments (F_4 and F_{10})

The differential equation for the twist angle θ of the beam (as demonstrated in Figure 3-4) is given by

$$F_4 = -GJ \frac{d\theta}{dx} \tag{3.11}$$

where GJ is the torsional stiffness. The integration of (3.11) gives

$$F_4 x = -GJ\theta + C_1 \tag{3.12}$$

By imposing $\theta=0$ at $x=l$ we evaluate the constant of integration

$$C_1 = F_4 l \tag{3.13}$$

Since $\theta=u_4$ at x=0, (3.12) and (3.13) result in

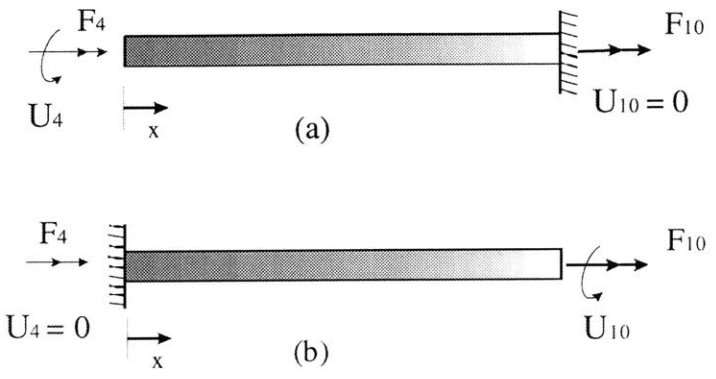

Figure 3-4: Twisting moments F4 and F10.

$$F_4 = \frac{GJ}{l} u_4 \tag{3.14}$$

From equilibrium of the twisting moments, we have

$$F_{10} = -F_4 \tag{3.15}$$

Therefore

$$k_{4,4} = \left(\frac{F_4}{u_4} \right) = \frac{GJ}{l} \tag{3.16}$$

and

$$k_{10,4} = \left(\frac{F_{10}}{u_4} \right) = -\frac{GJ}{l} \tag{3.17}$$

All other terms in the fourth column of the stiffness matrix are zero. In a similar way, if u_4=0, as demonstrated in Figure 3-4b, it can be shown that

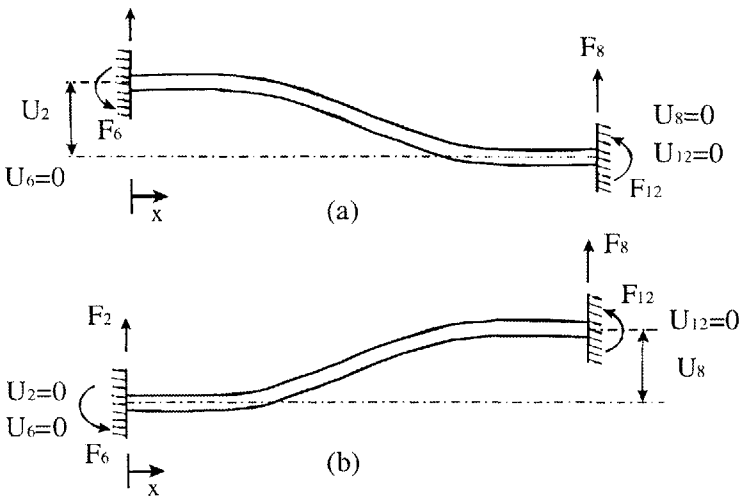

Figure 3-5: Shear forces F2 and F8.

$$k_{10,10} = \frac{GJ}{l} \tag{3.18}$$

• Shearing forces (F_2 and F_8)

The transverse displacement v of the beam, as demonstrated in Figure 3-5a is given by

$$v = v_b + v_s \tag{3.19}$$

where v_b is the transverse deflection due to bending and v_s is the deflection due to shear, governed by

$$\frac{dv_s}{dx} = -\frac{F_2}{GA_S} \tag{3.20}$$

where A_s is the effective cross-sectional area in shear. The bending deflection (shown in Figure 3-5a) is governed by the differential equation

$$EI_Z \frac{d^2 v_b}{dx^2} = F_2 x - F_6 \tag{3.21}$$

Integration and addition of equations (3-20) and (3-21) gives

$$EI_z v = \frac{F_2 x^3}{6} - \frac{F_6 x^2}{2} + (C_1 - \frac{F_2 EI_Z}{GA_S})x + C_2 \tag{3.22}$$

By imposing the boundary conditions given in Figure 3-5a we get

$$\frac{dv}{dx} = \frac{dv_s}{dx} = \frac{-F_2}{GA_S} \quad \text{at x=0, x=l} \tag{3.23}$$

$$v = 0 \text{ at } x=l \tag{3.24}$$

Substituting the values of C_1 and C_2 into (3.22) leads to

$$EI_Z v = \frac{F_2 x^3}{6} - \frac{F_6 x^2}{2} - \frac{F_2 \Phi x l^2}{12} + (1+\Phi)\frac{l^3 F_2}{12} \tag{3.25}$$

where

$$F_6 = \frac{F_2 l}{2} \tag{3.26}$$

and

$$\Phi = \frac{12EI_Z}{GA_S l^2} \tag{3.27}$$

From equilibrium we get

$$F_8 = -F_2 \tag{3.28}$$

and

$$F_{12} = -F_6 + F_2 l \tag{3.29}$$

Since at $x=0$ the transverse displacement is u_2, we have from (3.25) that

$$u_2 = (1+\Phi)\frac{l^3 F_2}{12EI_Z} \tag{3.30}$$

From Equations (3.26), (3.28), (3.29) and (3.30), we get

$$k_{2,2} = \left(\frac{F_2}{u_2}\right) = \frac{12EI_Z}{(1+\Phi)l^3} \tag{3.31}$$

$$k_{6,2} = \left(\frac{F_6}{u_2}\right) = \left(\frac{F_2 l}{2u_2}\right) = \frac{6EI_Z}{(1+\Phi)l^2} \tag{3.32}$$

$$k_{8,2} = \left(\frac{F_8}{u_2}\right) = \frac{-12EI_Z}{(1+\Phi)l^3} \tag{3.33}$$

$$k_{12,2} = \left(\frac{F_{12}}{u_2}\right) = \left(\frac{-F_6 + F_2 l}{u_2}\right) = \frac{6EI_Z}{(1+\Phi)l^2} \tag{3.34}$$

while all other terms in the second column are equal to zero. In a similar way, by fixing the left hand side of the beam, as demonstrated in Figure 3-5b, it can be shown that

$$k_{8,8} = k_{2,2} = \frac{12EI_Z}{(1+\Phi)l^3} \tag{3.35}$$

$$k_{12,8} = -k_{6,2} = \frac{-6EI_Z}{(1+\Phi)l^2} \tag{3.36}$$

• Bending moments (F_6 and F_{12})

Figure 3-6 shows the deformation caused to the beam by bending moments. The governing differential equation is again (3.22), but the constants C_1 and C_2 are now evaluated using different boundary conditions. Considering first the boundary condition shown in Figure 3-6a we have

$$v=0 \quad at \quad x=0,\ x=l \tag{3.37}$$

and

$$\frac{dv}{dx} = \frac{dv_S}{dx} = -\frac{F_2}{GA_S} \quad \text{at } x=l \tag{3.38}$$

As a result, Equation (3.22) becomes

$$EI_Z v = \frac{F_2}{6}(x^3 - l^2 x) + \frac{F_6}{2}(lx - x^2) \tag{3.39}$$

and

$$F_2 = \frac{6S_6}{(4+\Phi)l} \tag{3.40}$$

Using the equilibrium stated in (3.28) and (3.29), we have at x=0

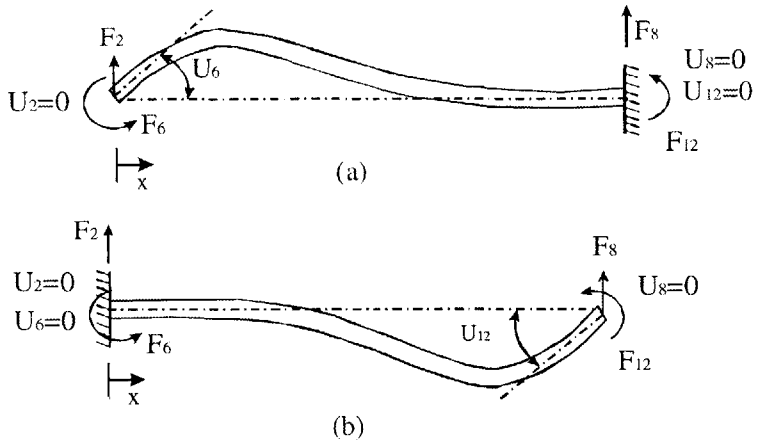

Figure 3-6: Bending moments F6 and F12.

$$\frac{dv_b}{dx} = \frac{dv}{dx} - \frac{dv_s}{dx} = u_6 \tag{3.41}$$

so that

$$u_6 = \frac{F_6(1+\Phi)l}{EI_Z(4+\Phi)} \tag{3.42}$$

Therefore, from equations (3.28), (3.29), (3.40) and (3.42) we get

$$k_{6,6} = \left(\frac{F_6}{u_6}\right) = \frac{(4+\Phi)EI_Z}{(1+\Phi)l} \tag{3.43}$$

$$k_{8,6} = \left(\frac{F_8}{u_6}\right) = \left(\frac{-F_2}{u_6}\right) = -\frac{6EI_Z}{(1+\Phi)l^2} \tag{3.44}$$

$$k_{12,6} = \left(\frac{F_{12}}{u_6}\right) = \left(\frac{-F_6 + F_2 l}{u_6}\right) = \frac{(2-\Phi)EI_Z}{(1+\Phi)l} \tag{3.45}$$

Using the boundary condition in Figure 3-6b and symmetry we obtain

$$k_{12,12} = k_{6,6} = \frac{(4+\Phi)EI_Z}{(1+\Phi)l} \tag{3.46}$$

The stiffness terms that correspond to the shear forces F_3 and F_9, and the bending moments F_5 and F_{11} can be obtained by derivations that are similar to those discussed above.

The complete stiffness matrix, as given in [16], can now be assembled, and it is given by

$$\begin{bmatrix} F_1 \\ F_2 \\ F_3 \\ F_4 \\ F_5 \\ F_6 \\ F_7 \\ F_8 \\ F_9 \\ F_{10} \\ F_{11} \\ F_{12} \end{bmatrix} = \begin{bmatrix} \frac{EA}{l} & & & & & & & & & & & \\ 0 & \frac{12EI_Z}{l^3(1+\Phi_Y)} & & & & & & & & & & \\ 0 & 0 & \frac{12EI_Y}{l^3(1+\Phi_Z)} & & & & & & & & & \\ 0 & 0 & 0 & \frac{GJ}{l} & & & & & & & & \\ 0 & 0 & \frac{-6EI_Y}{l^2(1+\Phi_Z)} & 0 & \frac{(4+\Phi_Z)EI_Y}{l(1+\Phi_Z)} & & & & & & & \\ 0 & \frac{6EI_Z}{l^2(1+\Phi_Y)} & 0 & 0 & 0 & \frac{(4+\Phi_Y)EI_Z}{l(1+\Phi_Y)} & & & & & & \\ \frac{-EA}{l} & 0 & 0 & 0 & 0 & 0 & \frac{AE}{l} & & & & & \\ 0 & \frac{-12EI_Z}{l^3(1+\Phi_Y)} & 0 & 0 & 0 & \frac{-6EI_Z}{l^2(1+\Phi_Y)} & 0 & \frac{12EI_Z}{l^3(1+\Phi_Y)} & & & & \\ 0 & 0 & \frac{-12EI_Y}{l^3(1+\Phi_Z)} & 0 & \frac{-6EI_Y}{l^2(1+\Phi_Z)} & 0 & 0 & 0 & \frac{12EI_Y}{l^3(1+\Phi_Z)} & & & \\ 0 & 0 & 0 & \frac{-GJ}{l} & 0 & 0 & 0 & 0 & 0 & \frac{GJ}{l} & & \\ 0 & 0 & \frac{-6EI_Y}{l^2(1+\Phi_Z)} & 0 & \frac{(2-\Phi_Z)EI_Y}{l(1+\Phi_Z)} & 0 & 0 & 0 & \frac{6EI_Y}{l^2(1+\Phi_Z)} & 0 & \frac{(4+\Phi_Z)EI_Y}{l(1+\Phi_Z)} & \\ 0 & \frac{6EI_Z}{l^2(1+\Phi_Y)} & 0 & 0 & 0 & \frac{(2-\Phi_Y)EI_Z}{l(1+\Phi_Y)} & 0 & \frac{-6EI_Z}{l^2(1+\Phi_Y)} & 0 & 0 & 0 & \frac{(4+\Phi_Y)EI_Z}{l(1+\Phi_Y)} \end{bmatrix} \begin{bmatrix} u_1 \\ u_2 \\ u_3 \\ u_4 \\ u_5 \\ u_6 \\ u_7 \\ u_8 \\ u_9 \\ u_{10} \\ u_{11} \\ u_{12} \end{bmatrix}$$

Symmetric

(3.47)

where

$$\Phi_Y = \frac{12EI_Z}{GA_{Sy}l^2} = 24(1+\upsilon)\frac{A}{A_{Sy}}\left(\frac{r_Z}{l}\right)^2 \tag{3.48}$$

and

$$\Phi_Z = \frac{12EI_Y}{GA_{Sz}l^2} = 24(1+\upsilon)\frac{A}{A_{Sz}}\left(\frac{r_y}{l}\right)^2 \tag{3.49}$$

are shear deformation terms. Note that r_z and r_y are the radiuses of gyration of the cross-section, and given by

$$r_Z = \sqrt{\frac{I_Z}{A}} \tag{3.50}$$

$$r_Y = \sqrt{\frac{I_Y}{A}} \tag{3.51}$$

If r_z/l and r_y/l are small relative to unity, as is the case with a thin beam, we can neglect the shear deformation and hence the terms Φ_Y and Φ_Z in (3.47) are set to zero.

3.1.3 Iso-beam element

The iso-beam element is formulated by using the virtual work principle with functions that approximate the actual displacements. As a result, the differential equations of equilibrium are not satisfied exactly, but the error reduces as the mesh is refined.

In the following we describe the formulation of the iso-beam element, as given in [2]. The formulation of the iso-beam element is derived using the principle of virtual work discussed above. This is demonstrated below using a simple case of a two-dimensional element with rectangular cross section, as shown in 3-7. The beam is subjected to transverse loading p and moment loading m, both per unit length. Applying the principle of virtual work with the assumptions discussed in section 3.1.1 we get:

$$EI\int_0^L(\frac{d\beta}{dx})(\frac{d\overline{\beta}}{dx})dx+GAk\int_0^L(\frac{dw}{dx}-\beta)(\frac{d\overline{w}}{dx}-\overline{\beta})dx=\int_0^L p\overline{w}\,dx+\int_0^L m\overline{\beta}dx \tag{3.52}$$

We obtain the element stiffness matrix by using the method of iso-parametric formulation discussed in Chapter 2, and by using the relations

$$w=\sum_{i=1}^{q}h_i w_i\,;\qquad \beta=\sum_{i=1}^{q}h_i\theta_i \tag{3.53}$$

where h_i are the interpolation functions given in Figure 3-8 and q is the number of the nodes. We define

$$w=H_w\hat{u}\,;\quad \beta=H_\beta\hat{u} \tag{3.54}$$

$$\frac{\partial w}{\partial x}=B_w\hat{u}\,;\quad \frac{\partial\beta}{\partial x}=B_\beta\hat{u} \tag{3.55}$$

where

$$\overline{\hat{u}}=[w_1...w_q\ \ \theta_1...\theta_q]$$

$$H_w=[h_1...h_q\ \ 0...0] \tag{3.56}$$

$$H_\beta=[0...0\ \ h_1...h_q]$$

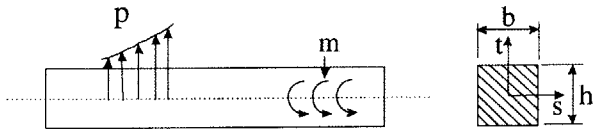

(a) Beam with applied loading

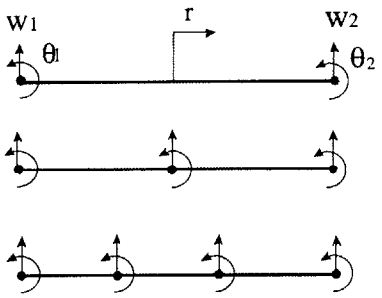

(b) 2-, 3- and 4- node iso-beam elements

Figure 3-7: Formulation of two-dimensional iso-beam element.

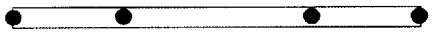

Node 1	Node 3	Node 4	Node 2	
r = -1	r = 0		r = +1	3-node case
r = -1	r = -1/3	r = 1/3	r = +1	4-node case

(a) 2 to 4 variable- number - nodes element

	include only if node 3 is present	include only if nodes 3 and 4 are present
$h_1 = \frac{1}{2}(1-r)$	$-\frac{1}{2}(1-r^2)$	$+\frac{1}{16}(-9r^3+r^2+9r-1)$
$h_2 = \frac{1}{2}(1+r)$	$-\frac{1}{2}(1-r^2)$	$+\frac{1}{16}(9r^3+r^2-9r-1)$
$h_3 = (1-r^2)$		$+\frac{1}{16}(27r^3+7r^2-27r-7)$
$h_4 = \frac{1}{16}(-27r^3-9r^2+27r+9)$		

(b) interpolation functions

Figure 3-8: Interpolation functions of two to four variable-number-nodes one-dimensional element (taken from [2]).

and

$$B_w = J^{-1}[\frac{\partial h_1}{\partial r} \ldots \frac{\partial h_q}{\partial r} \quad 0 \ldots 0]$$
$$B_\beta = J^{-1}[0 \ldots 0 \quad \frac{\partial h_1}{\partial r} \ldots \frac{\partial h_q}{\partial r}] \tag{3.57}$$

where $J = \frac{\partial x}{\partial r}$. Using the above definitions we can construct the element stiffness matrix

$$K = EI \int_{-1}^{1} B_\beta^T B_\beta \det J \, dr + GAk \int_{-1}^{1} (B_w - H_\beta)^T (B_w - H_\beta) \det J \, dr \tag{3.58}$$

3.1.4 Comparison between Hermitian and iso-beam elements

Since both the isoparametric beam and the Hermitian beam elements can be used to model beam structures, we may ask which element should be preferred. It is clear that in the case of linear analysis of straight beams the Hermitian elements are more cost-effective, since they can describe cubic variations of displacements with half the degrees of freedom. However, the isoparametric beam element predicts the shear deformation more accurately, and enables a natural representation of curved beams. In the analyses of stiffened plates and shells the use of isoparametric elements may be effective, since the number of nodes along the isoparametric beam can be set to fit the number of nodes on the shell element edge (when the 4-, 8- or 16-node shell element is employed, the isoparametric element is employed with 2,3 and 4 nodes).

3.2 Shell elements

During the course of this research work, shell elements were used extensively, both in the "all-shell" models, where only shell elements are present, and in hybrid models, where the shell elements are assembled with different types of beam elements.

In the various finite elements models that were constructed and solved, we used *flat* rectangular shell elements, which are a special case of the general curved shell element. Therefore, we shall limit the discussion about the mechanics and formulation of the shell elements to the special case of flat rectangular elements.

In the following we describe the formulation of a flat shell element using the approach given in [2]. A simple rectangular flat shell element can be obtained by superimposing the plate bending behavior and the plane stress behavior. This superposition and the resulting element are shown in Figure 3-9. We designate the bending stiffness matrix of the element as $\tilde{K}_B$ and the membrane stiffness matrix as $\tilde{K}_M$. Using these matrices we can assemble the total stiffness matrix

$$\underset{20X20}{\tilde{K}_S} = \begin{bmatrix} \underset{12X12}{\tilde{K}_B} & 0 \\ 0 & \underset{8X8}{\tilde{K}_M} \end{bmatrix} \tag{3-59}$$

The formulation of the matrices $\tilde{K}_B$ and $\tilde{K}_M$ is discussed in the following. We start with the iso-parametric formulation of $\tilde{K}_B$, which is basically the stiffness of a plate element.

• Iso-parametric formulation of a plate element

The formulation of the plate element is based on the plate theory by E. Reissner and R.D. Mindlin, which includes shear deformation. According to this theory, material

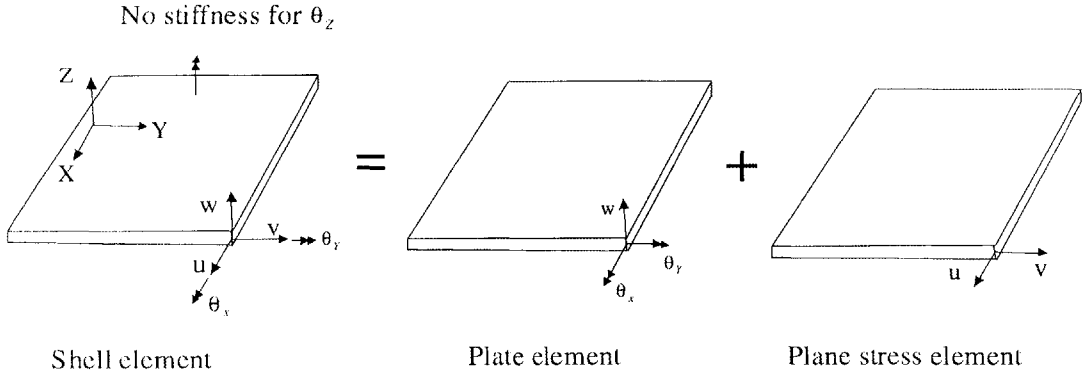

Figure 3-9: Flat shell element - superposition of a plate element and a plan stress element.

particles that were on a straight line, perpendicular to the mid-surface of the undeformed plate, remain on a straight line during deformation, although this line is no longer normal to the deformed mid-surface. As a result, we can state the displacement of the material particles to be as follows

$$u = -z\beta_x(x,y); \quad v = -z\beta_y(x,y); \quad w = w(x,y) \tag{3.60}$$

where w is the lateral deflection, β_x is the rotation of the normal to the mid-surface in the x,z plane and β_y is the rotation in the y,z plane, as demonstrated in Figure 3-10.

The bending strains $\varepsilon_{xx}, \varepsilon_{yy}, \gamma_{xy}$ vary linearly through the plate thickness and are given by

$$\begin{bmatrix} \varepsilon_{xx} \\ \varepsilon_{yy} \\ \gamma_{xy} \end{bmatrix} = -z \begin{bmatrix} \partial\beta_x / \partial x \\ \partial\beta_y / \partial y \\ \dfrac{\partial\beta_x}{\partial y} + \dfrac{\partial\beta_y}{\partial x} \end{bmatrix} \tag{3.61}$$

while the transverse shear strains, which are constant across the thickness, are given by

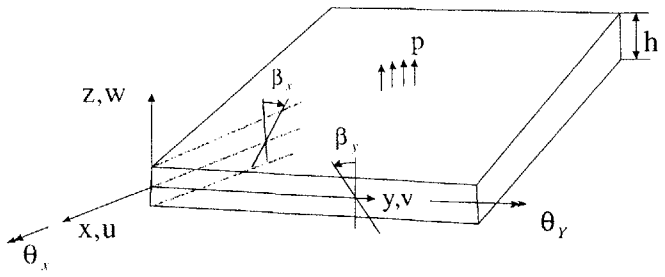

Figure 3-10: Deformation assumptions in analysis of plate including shear deformation.

$$\begin{bmatrix}\gamma_{xz}\\ \gamma_{yz}\end{bmatrix}=\begin{bmatrix}\dfrac{\partial w}{\partial x}-\beta_x\\ \dfrac{\partial w}{\partial y}-\beta_y\end{bmatrix} \tag{3.62}$$

Since the normal stress in the z direction is zero, we have a plane stress condition. For this case, the relations between the stresses and strains, provided that the material is isotropic, are

$$\begin{bmatrix}\tau_{xx}\\ \tau_{yy}\\ \tau_{xy}\end{bmatrix}=-z\frac{E}{1-\upsilon^2}\begin{bmatrix}1 & \upsilon & 0\\ \upsilon & 1 & 0\\ 0 & 0 & \dfrac{1-\upsilon}{2}\end{bmatrix}\begin{bmatrix}\partial\beta_x/\partial x\\ \partial\beta_y/\partial y\\ \dfrac{\partial\beta_x}{\partial y}+\dfrac{\partial\beta_x}{\partial y}\end{bmatrix} \tag{3.63}$$

$$\begin{bmatrix}\tau_{xz}\\ \tau_{yz}\end{bmatrix}=\frac{E}{2(1+\upsilon)}\begin{bmatrix}\dfrac{\partial w}{\partial x}-\beta_x\\ \dfrac{\partial w}{\partial y}-\beta_y\end{bmatrix} \tag{3.64}$$

For a plate loaded with a force per unit area, p, the principle of virtual work takes the form

$$\int_A \int_{-\frac{h}{2}}^{\frac{h}{2}} [\bar{\varepsilon}_{xx} \;\; \bar{\varepsilon}_{yy} \;\; \bar{\gamma}_{xy}] \begin{bmatrix} \tau_{xx} \\ \tau_{yy} \\ \tau_{xy} \end{bmatrix} dz\, dA + k \int_A \int_{-\frac{h}{2}}^{\frac{h}{2}} [\bar{\gamma}_{xz} \;\; \bar{\gamma}_{yz}] dz\, dA = \int_A \bar{w}\, p\, dA \tag{3.65}$$

where the terms designated with the overbar stand for virtual quantities, and k is a constant used to obtain the effective shear area. By substituting (3.71) to (3.74) into (3.75), we get

$$\int_A \bar{\kappa}^T C_b \kappa\, dA + \int_A \bar{\gamma}^T C_S \gamma\, dA = \int_A \bar{w}\, p\, dA \tag{3.66}$$

where $C_b\kappa$ are the internal bending moments, $C_S\gamma$ are the shear forces and

$$\kappa = \begin{bmatrix} \partial\beta_x / \partial x \\ \partial\beta_y / \partial y \\ \dfrac{\partial\beta_x}{\partial y} + \dfrac{\partial\beta_y}{\partial x} \end{bmatrix} \tag{3.67}$$

$$\gamma = \begin{bmatrix} \dfrac{\partial w}{\partial x} - \beta_x \\ \dfrac{\partial w}{\partial y} - \beta_y \end{bmatrix} \tag{3.68}$$

$$C_b = \frac{Eh^3}{12(1-\upsilon^2)} \begin{bmatrix} 1 & \upsilon & 0 \\ \upsilon & 1 & 0 \\ 0 & 0 & \dfrac{1-\upsilon}{2} \end{bmatrix} \tag{3.69}$$

$$C_S = \frac{Ehk}{2(1+\upsilon)} \begin{bmatrix} 1 & 0 \\ 0 & 1 \end{bmatrix} \tag{3.70}$$

We use the following displacement relations

$$w = \sum_{i=1}^{q} h_i w_i ; \quad \beta_x = -\sum_{i=1}^{q} h_i \theta_y^i ; \quad \beta_y = \sum_{i=1}^{q} h_i \theta_x^i \tag{3.71}$$

where q is the number of nodes and the interpolation functions (h_i) are given in Figure 3-11 for various number of nodes per element.

By letting

$$\kappa(r,s) = B_\kappa \hat{u} \tag{3.72}$$

$$\gamma(r,s) = B_\gamma \hat{u} \tag{3.73}$$

$$w(r,s) = H_w \hat{u} \tag{3.74}$$

where

$$\hat{u} = [w_1, \theta_x^1, \theta_y^1 ; w_2 \ldots \theta_y^q] \tag{3.75}$$

and using (3.67) to (3.75) we obtain the stiffness matrix of the plate element:

$$K = \int_{-1}^{+1}\int_{-1}^{+1} (B_\kappa^T C_b B_\kappa + B_\gamma^T C_S B_\gamma)\, dr\, ds \det J \tag{3.76}$$

As stated in (3.59), the stiffness matrix of a flat shell element can be constructed by superimposing the plate bending and plane stress behaviors. We shall now complete the formulation of the flat shell element by description of the derivation of $\tilde{K}_M$, the stiffness matrix of a plane stress element (also referred to as membrane element). This derivation also serves as an explicit demonstration of the isoparametric formulation method.

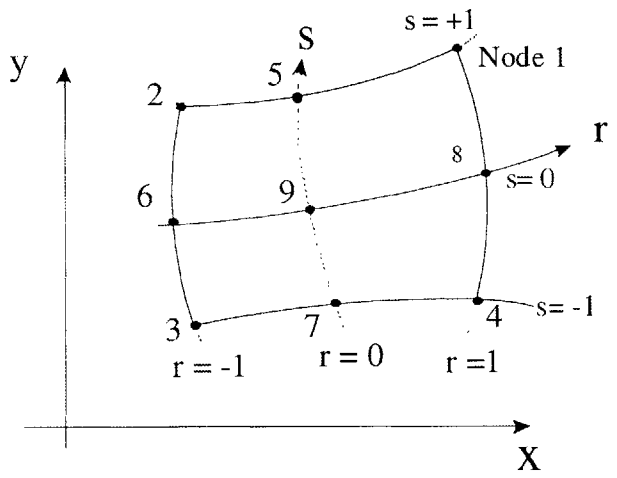

(a) 4 to 9 variable-number-nodes two dimensional element

h_1	$\frac{1}{4}(1+r)(1+s)$	$-\frac{1}{2}h_5$			$-\frac{1}{2}h_8$	$-\frac{1}{4}h_9$
h_2	$\frac{1}{4}(1-r)(1+s)$	$-\frac{1}{2}h_5$	$-\frac{1}{2}h_6$			$-\frac{1}{4}h_9$
h_3	$\frac{1}{4}(1-r)(1-s)$		$-\frac{1}{2}h_6$	$-\frac{1}{2}h_7$		$-\frac{1}{4}h_9$
h_4	$\frac{1}{4}(1+r)(1-s)$			$-\frac{1}{2}h_7$	$-\frac{1}{2}h_8$	$-\frac{1}{4}h_9$
h_5	$\frac{1}{2}(1-r^2)(1+s)$					$-\frac{1}{2}h_9$
h_6	$\frac{1}{2}(1-s^2)(1-r)$					$-\frac{1}{2}h_9$
h_7	$\frac{1}{2}(1-r^2)(1-s)$					$-\frac{1}{2}h_9$
h_8	$\frac{1}{2}(1-s^2)(1+r)$					$-\frac{1}{2}h_9$
h_9	$(1-r^2)(1-s^2)$					

(b) Interpolation functions

Figure 3-11: Interpolation functions of four to nine variable-number-nodes two-dimensional element (taken from [2]).

• Iso-parametric formulation of plane stress element.

For simplicity we derive the stiffness matrix of the 4-node two-dimensional element, described in Figures 3-12. The derivation is based on the approach given in [2]. The coordinate interpolation functions (using the 4-node element case in Figure 3-11) are given by

$$x=\frac{1}{4}(1+r)(1+s)x_1+\frac{1}{4}(1-r)(1+s)x_2+\frac{1}{4}(1-r)(1-s)x_3+\frac{1}{4}(1+r)(1-s)x_4$$

$$y=\frac{1}{4}(1+r)(1+s)y_1+\frac{1}{4}(1-r)(1+s)y_2+\frac{1}{4}(1-r)(1-s)y_3+\frac{1}{4}(1+r)(1-s)y_4 \quad (3.77)$$

Similarly, the displacement interpolation functions are

$$u=\frac{1}{4}(1+r)(1+s)u_1+\frac{1}{4}(1-r)(1+s)u_2+\frac{1}{4}(1-r)(1-s)u_3+\frac{1}{4}(1+r)(1-s)u_4$$

$$v=\frac{1}{4}(1+r)(1+s)v_1+\frac{1}{4}(1-r)(1+s)v_2+\frac{1}{4}(1-r)(1-s)v_3+\frac{1}{4}(1+r)(1-s)v_4 \quad (3.78)$$

The strains that correspond to the element degrees of freedom are

$$\varepsilon^T=[\varepsilon_{xx}\ \varepsilon_{yy}\ \gamma_{xy}] \quad (3.79)$$

where

$$\varepsilon_x=\frac{\partial u}{\partial x};\quad \varepsilon_y=\frac{\partial v}{\partial y};\quad \gamma_{xy}=\frac{\partial u}{\partial y}+\frac{\partial v}{\partial x} \quad (3.80)$$

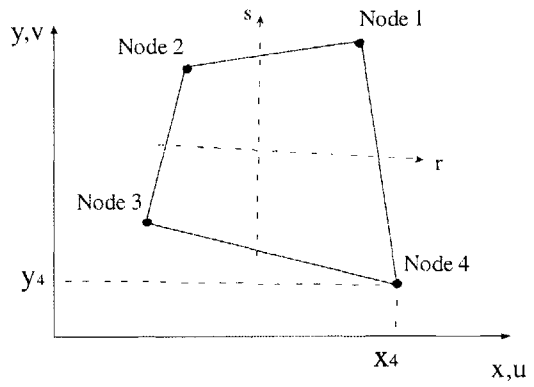

Figure 3-12: Four node two-dimensional element.

The displacement derivatives are obtained by:

$$\begin{bmatrix} \frac{\partial}{\partial r} \\ \frac{\partial}{\partial s} \end{bmatrix} = \begin{bmatrix} \frac{\partial x}{\partial r} & \frac{\partial y}{\partial r} \\ \frac{\partial x}{\partial s} & \frac{\partial y}{\partial s} \end{bmatrix} \begin{bmatrix} \frac{\partial}{\partial x} \\ \frac{\partial}{\partial y} \end{bmatrix} \tag{3.81}$$

or in shorter form

$$\frac{\partial}{\partial r} = J \frac{\partial}{\partial x} \tag{3.82}$$

where

$$\frac{\partial x}{\partial r} = \frac{1}{4}(1+s)x_1 - \frac{1}{4}(1+s)x_2 - \frac{1}{4}(1-s)x_3 + \frac{1}{4}(1-s)x_4$$

$$\frac{\partial x}{\partial s} = \frac{1}{4}(1+r)x_1 + \frac{1}{4}(1-r)x_2 - \frac{1}{4}(1-r)x_3 - \frac{1}{4}(1+r)x_4$$

$$\frac{\partial y}{\partial r} = \frac{1}{4}(1+s)y_1 - \frac{1}{4}(1+s)y_2 - \frac{1}{4}(1-s)y_3 - \frac{1}{4}(1-s)y_4$$

$$\frac{\partial y}{\partial s}=\frac{1}{4}(1+r)y_1+\frac{1}{4}(1-r)y_2-\frac{1}{4}(1-r)y_3-\frac{1}{4}(1+r)y_4 \tag{3.83}$$

To strains are obtained by

$$\frac{\partial u}{\partial r}=\frac{1}{4}(1+s)u_1-\frac{1}{4}(1+s)u_2-\frac{1}{4}(1-s)u_3+\frac{1}{4}(1-s)u_4$$

$$\frac{\partial u}{\partial s}=\frac{1}{4}(1+r)u_1+\frac{1}{4}(1-r)u_2-\frac{1}{4}(1-r)u_3-\frac{1}{4}(1+r)u_4$$

$$\frac{\partial v}{\partial r}=\frac{1}{4}(1+s)v_1-\frac{1}{4}(1+s)v_2-\frac{1}{4}(1-s)v_3-\frac{1}{4}(1-s)v_4$$

$$\frac{\partial v}{\partial s}=\frac{1}{4}(1+r)v_1+\frac{1}{4}(1-r)v_2-\frac{1}{4}(1-r)v_3-\frac{1}{4}(1+r)v_4 \tag{3.84}$$

consequently,

$$\begin{bmatrix}\frac{\partial u}{\partial x}\\ \frac{\partial u}{\partial y}\end{bmatrix}=\frac{1}{4}J^{-1}\begin{bmatrix}1+s & 0 & -(1+s) & 0 & -(1-s) & 0 & 1-s & 0\\ 1+r & 0 & 1-r & 0 & -(1-r) & 0 & -(1+r) & 0\end{bmatrix}\hat{u} \tag{3.85}$$

and

$$\begin{bmatrix}\frac{\partial v}{\partial x}\\ \frac{\partial v}{\partial y}\end{bmatrix}=\frac{1}{4}J^{-1}\begin{bmatrix}0 & 1+s & 0 & -(1+s) & 0 & -(1-s) & 0 & 1-s\\ 0 & 1+r & 0 & 1-r & 0 & -(1-r) & 0 & -(1+r)\end{bmatrix}\hat{u} \tag{3.86}$$

where

$$\hat{u} = [u_1\ v_1\ u_2\ v_2\ u_3\ v_3\ u_4\ v_4] \tag{3.87}$$

Using the relations in (3.85) and (3.86) we can establish the strain-displacement transformation matrix B:

$$B = \frac{1}{4} J^{-1} \begin{bmatrix} 1+s & 0 & -(1+s) & 0 & -(1-s) & 0 & 1-s & 0 \\ 0 & 1+r & 0 & 1-r & 0 & -(1-r) & 0 & -(1+r) \\ 1+r & 1+s & 1-r & -(1+s) & -(1-r) & -(1-s) & -(1+r) & 1-s \end{bmatrix} \tag{3.88}$$

and the stiffness matrix is then given by

$$K = \int_{r=-1}^{1} \int_{s=-1}^{1} B^T C B t \det J \, dr \, ds \tag{3.89}$$

where t is the element thickness, and C is the stress-strain matrix for plane stress condition:

$$C = \frac{E}{1-\nu^2} \begin{bmatrix} 1 & \nu & 0 \\ \nu & 1 & 0 \\ 0 & 0 & \frac{1-\nu}{2} \end{bmatrix} \tag{3.90}$$

4 A study of element modeling capabilities: analysis of cantilever beams

4.1 The purpose of this study

In order to gain insight into the modeling capabilities of the different elements, various simple models of beams were constructed and solved. The conclusions obtained by the solution of these simple models were found valuable for the analysis of the stiffened plate structure.

The demonstrating models included the cantilever beams with "I" and "T" cross-sections, described in Figure 4-1. The beams were subjected to bending and torque by means of a concentrated force and a concentrated moment at the tip. The analysis included the solution of deflections and stresses.

First, a three-dimensional model was constructed and solved, in order to obtain a reference solution. This model's solution was compared to the well-known analytical solutions by Bernoulli and Timoshenko. Then, the other modeling methods were examined by comparison to the three-dimensional model. The next step was to investigate the influence of the depth of the web on the performance of the different models.

Different cross-section types ("T" and "I") were used in order to see whether the conclusions about the modeling capabilities would be valid for more general cases. The "T" cross-section is more attractive since its components, the web and the flange, resemble the components of the stiffened plate: the stiffener and the effective breadth of the plate, above each stiffener. However, the experiments using both types of cross-sections yielded the same conclusions about the modeling capabilities.

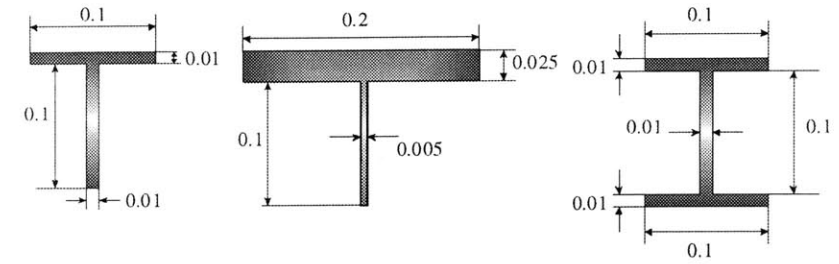

4-1a
T cross-section no 1

4-1b
T cross-section no 2

4-1c
I cross-section

All dimensions are in meters.
Length of all beams: 1 [m]

Figure 4-1: Cross-sections of cantilever beams under investigation.

4.2 Finite elements models.

The "T" beam was modeled using four different methods, as described in Figure 4-2. The formulation of the various elements is discussed in Chapter 3. The following is a description of the models, by decreasing order of mathematical hierarchy:

1). "Three-dimensional model" – constructed from solid elements with 20 nodes per element. The three-dimensional model is the most comprehensive of all mathematical models. The major disadvantage of the usage of the three-dimensional model is the cost in computer resources. For many engineering problems the usage of less comprehensive models will be adequate, and there is no need to use three-dimensional solid elements.

2). "All shell model" – constructed from 8-node shell elements.

3). "Iso beam model" – a combination of 3-node iso-beam elements with 8-node shell elements. The Iso-beam element nodes are connected to the shell element nodes by means of rigid links. Rigid links are special constraint equations between two nodes – a master node and a slave node. As the nodes displace due to deformation, the slave node is constrained to translate and rotate such that the distance between the master node and the slave node remains constant, and that the rotations at the slave node are the same as the corresponding rotations at the master node.

4). "Hermitian beam model" – a combination of a Hermitian beam element (2-nodes per element by definition of the Hermitian beam element) and 4-node shell elements. The

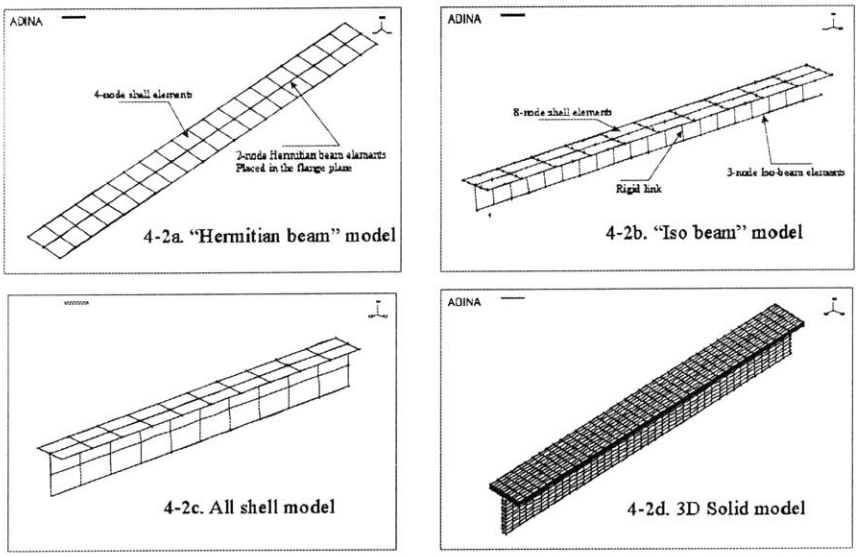

Figure 4-2: Finite element models of cantilever beam with a "T" cross-section.

low order (4-node) shell elements were used in order to have compatibility (as per the nodes, but not by the displacement functions) with the 2-node Hermitian beam elements. The Hermitian beam elements are in the flange plane, and hence are sharing the nodes of the shell elements. The fact that the web is eccentric to the flange surface is taken care of by definition of an offset value.

The "I" cross-section beam served to further investigate particular issues, as described below, and was modeled using the "all-shell" and the "Iso-beam" methods.

4.3 Summary of results

A bending load case (applied by a tip force) was solved using the various modeling methods. This load case solution was the basis for the evaluation of the various models. First, the cross-section described in Figure 4-1a was modeled. This beam will be referred to below as the "reference beam". Then, a further investigation on the influence of the web depth was conducted. Displacement and stresses (both axial and shear) were studied using each model.

We begin the results summary with the three-dimensional solution. This solution, together with some analytical results, will be used for the evaluation of the other modeling methods.

4.3.1 Three-dimensional model – the reference solution

As mentioned above, the reference beam was analyzed with a tip load. Figure 4-3 describes the comparison of the three-dimensional solution with the well-known solutions based on Bernoulli and Timoshenko beam theory.

The analytical beam theory solutions do not coincide with the three-dimensional solution (which is a better representation of the real beam): the Bernoulli beam is too rigid, while the Timoshenko beam is too flexible. The discrepancies are due to the assumptions involved with these theories. Bernoulli's classic beam theory does not account for deflections due to shear strain, and assumes that planes originally normal to the neutral axis remain plane and normal during deformation. This assumption introduces a constraint that does not exist in reality.

The Timoshenko theory, which includes (in a simplified manner) deflections caused by shear strain, assumes that planes remain plane, but no longer normal to the neutral axis. The latter assumption relaxes the constraint used in the Bernoulli theory. The Timoshenko theory yields slightly larger displacements than the three-dimensional model, since it does not include the three-dimensional material effect (Poisson's effect) near the fixed end of the beam. It should be noted that this is true also for the Bernoulli beam theory, which nevertheless yields smaller deflections than the three-dimensional model

4.3.2 Hermitian beam model

4.3.2.1 Predicted displacements

Figure 4-4 describes the deflection of the reference beam, subjected to the tip load. It can be seen that the Hermitian beam model solution (marked as the "original Hermitian

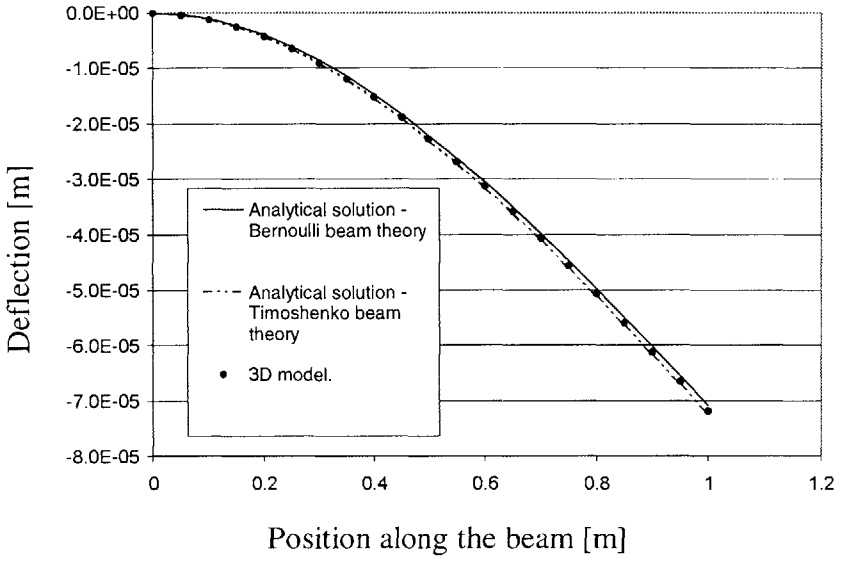

Figure 4-3: Bending deflection of beam with "T" cross-section, comparison of 3D model solution to analytical beam theory solution.

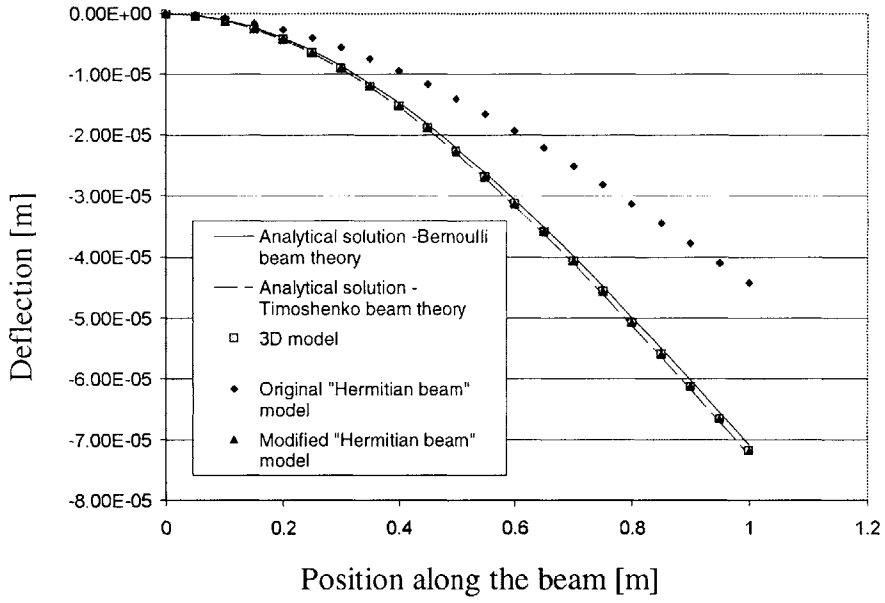

Figure 4-4: Deflection of a "T" beam – original and modified Hermitian beam models.

model") yields substantially smaller deflections than the three-dimensional solution. The reason for it lies in the nature of the model's definition, as explained below.

As demonstrated in Figure 4-2a, the Hermitian beam elements are placed in the plane of the shell elements. The fact that the actual beam in the real structure is eccentric (located on one side of the plate) is taken into account by a definition of an offset value. The apparently natural definition of the offset value is the distance between the mid-surface of the plate and the centroid of the web, as demonstrated in Figure 4-5a (noted as $d_{original}$). Although it seems natural, this definition of the offset will result in an erroneous representation of the beam (too-rigid model) *since the fibers of the cross-section represented by the Hermitian beam and the shell elements will bend about the midsurface of the plate and not about the real neutral axis of the cross- section*, which is somewhere in-between the midsurface of the plate and the centroid of the web. Hence, when the use of the Hermitian beam is considered, the offset of the beam centroid from the location of the nodes should be adjusted such that the combination of the elements will yield the real moment of inertia. This value of offset should be calculated separately, as explained below.

Since the moments of inertia of the flange and the web are well modeled by the elements, the offset value should be calculated in such a way that it compensates for the fact that *both the flange and the web* are bent about an axis that is not their own centroids. We shall now derive the expression for the modified offset.

The moment of inertia of the cross section is given as:

$$I_{total} = I_1 + A_1 \cdot d_1^{\,2} + I_2 + A_2 \cdot d_2^{\,2} \tag{4.1}$$

where I_1 and I_2 are the moments of inertia of the web and the flange respectively, about their own centroids. The definitions of A_1, A_2, d_1 and d_2 are given in Figure 4-5.

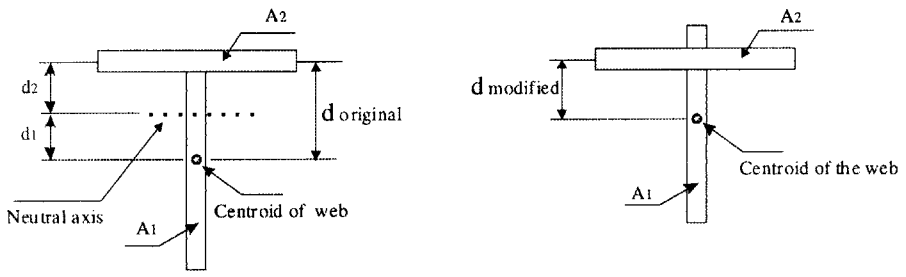

Original Hermitian beam cross-section 4-5a

Modified Hermitian beam cross-section 4-5b

Figure 4-5: Original and modified Hermitian beam models – definition of cross-section.

The definition of the "original" Hermitian model, as described above, leads to a moment of inertia that is equivalent to:

$$I_{total} = I_1 + I_2 + A_1 \cdot (d_{original})^2 \tag{4.2}$$

where the definition of $d_{original}$ is given in Figure 4-5a. The expression in (4.2) is clearly different from the one given in (4.1), and hence needs to be adjusted. The adjustment is done by a variation of the offset value, namely, by deriving a modified value of the offset such that the expressions in (4.1) and (4.2) will yield the same result. By equating (4.1) and (4.2) and dropping identical terms from both sides we get:

$$A_1 \cdot (d_{modified})^2 = A_1 \cdot d_1^{\,2} + A_2 \cdot d_2^{\,2} \tag{4.3}$$

The solution for $d_{modified}$ from equation (4-3) yields:

$$d_{modified} = \sqrt{\frac{A_1 \cdot d_1^{\,2} + A_2 \cdot d_2^{\,2}}{A_1}} \tag{4.4}$$

This way, we obtain a value that is smaller than the actual distance between the mid-surface of the plate and the centroid of the web. Once the adjusted offset value is entered into the model, the results are close to those obtained using the three-dimensional model and the analytical beam theories (see Figure 4-4).

4.3.2.2 Predicted stresses

Figure 4-6 depicts the bending stress in the reference beam, at the bottom of the web. It can be noted that the original Hermitian model yielded substantially smaller stresses than the three-dimensional model or the analytical beam theory solution (maximum error of –38.5%, relatively to three-dimensional model). Once the Hermitian model was defined using the adjusted offset, the correct stresses were obtained.

Figure 4-7 depicts the shear stress due to bending in the web of the reference beam. It can be seen that the Hermitian beam models (both the original and the modified models) yield a constant shear stress across the web, as opposed to the quadratic analytical solution pattern (which is also observed in the three-dimensional and all shell models). Furthermore, the Hermitian models do not predict correctly the distribution of the shear force over the whole cross-section area. They predict that about 75.9% of the shear force is carried by the web, while the analytical solution gives a value of 93.4%.

We can conclude that the assumption of constant shear stress in the Hermitian beam element (see derivation of the element formulation in Section 3.1.2) leads to erroneous shear force (and hence stress) prediction in the stiffeners.

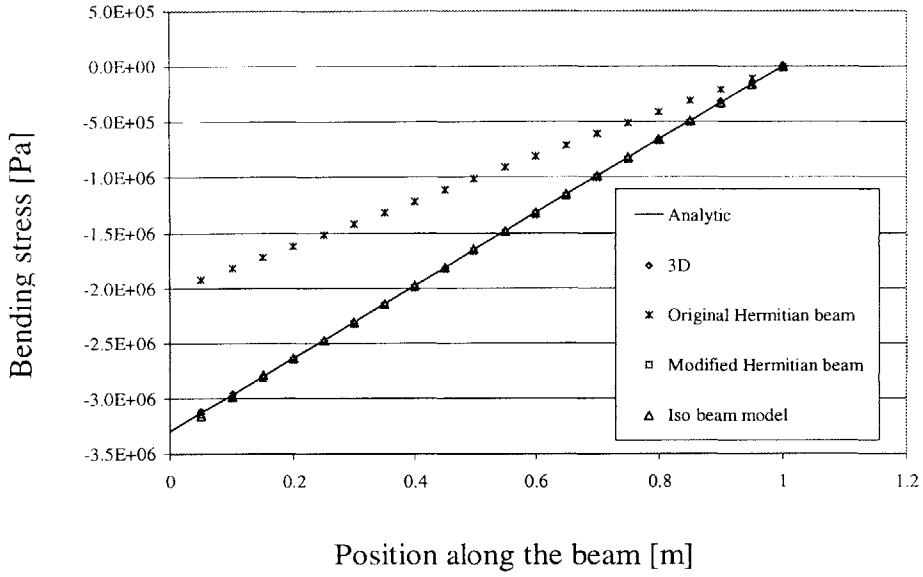

Figure 4-6: Bending stresses in "T" cross-section beam.

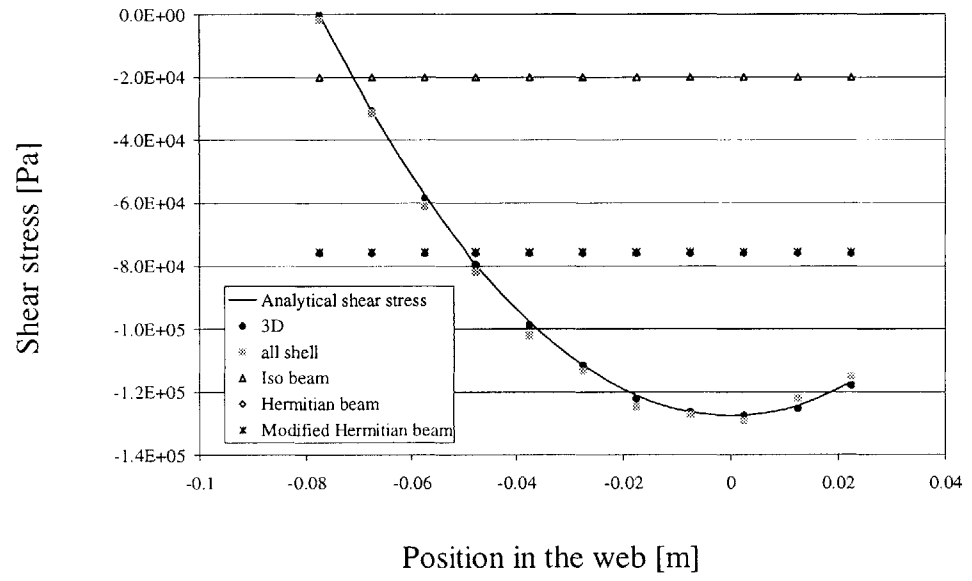

Figure 4-7: Shear stress due to bending in a web of a "T" cross-section beam.

4.3.3 Iso beam model

4.3.3.1 Predicted displacements

As opposed to the Hermitian beam model, the iso-beam model does not use an offset definition. Instead, the iso-beam element nodes lie on a line located at the natural axis of the web. The displacements predicted by the iso-beam element model are very close to those obtained by the three-dimensional model – see Figure 4-4.

4.3.3.2 Evaluation of stresses

The bending stresses, as obtained by the iso-beam model, are very close to the three-dimensional and analytical solutions, as described in Figure 4-6.

Similar to the Hermitian model, the iso-beam model predicts an erroneous constant shear stress pattern in the web (see Figure 4-7). This leads to a wrong shear force taken by the web: 20.3% of the total shear force instead of 93.4% obtained by the analytical solution. We can conclude that the rigid link connection between the shell elements and the iso beam elements cannot model correctly the distribution of shear force over the cross section.

This error, in predicting the shear force distribution repeats for the "I" cross-section case, where the iso-beam model predicts that 65.9% of the shear force is carried by the web, while the analytical solution gives that 91.6% of the force is carried by the web.

4.3.4 All shell model

4.3.4.1 Predicted displacements

In general, the construction of a model of a beam of arbitrary cross-section using only shell elements, results in a geometric error due to the overlapping that occurs in the intersection between the shell elements. This applies for the "T" cross-section, as can be seen in Figure 4-8. The analyst may approach the problem by several ways, as described below.

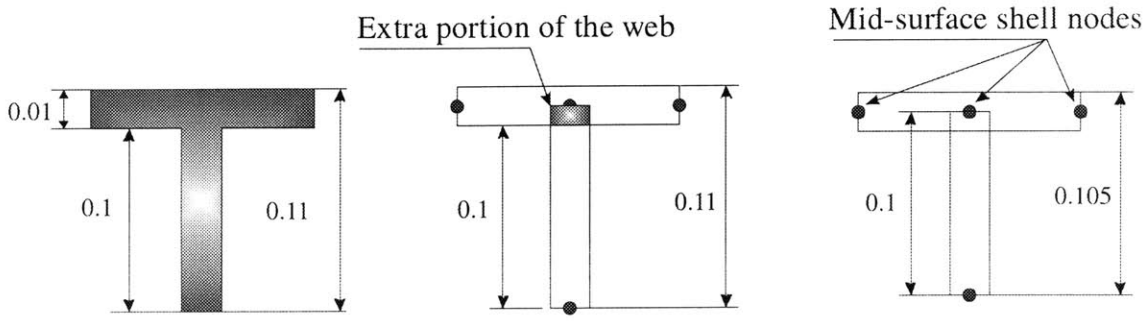

Real cross-section
4-8a

All-shell model
"too-rigid" cross-section
4-8b

All-shell model
"too-flexible" cross-section
4-8c

Figure 4-8: "All-shell" models of a beam with "T" cross-section.

- Cross-section definition – approach no. 1.

The first approach, which is most likely used, is depicted in Figure 4.8b and results into a "too rigid" cross-section. In this approach, the depth of the web is defined as the real web depth plus half of the plate thickness. The model is then *too rigid*, due to the extra segment of the web in the overlapping area, and hence smaller deflections are predicted. The error is relatively small: about 1.3% of discrepancy from the three-dimensional solution (see Figure 4-9).

- Cross-section definition – approach no. 1 – influence of the web's depth.

The discrepancies of the "too rigid" model relatively to the three-dimensional model vary with the depth of the web, diminishing as the web depth approaches very large values. This follows from the fact that the error of having an extra portion of the web inside the half thickness of the plate has a negligible contribution to the total moment of inertia, when the web depth is very large. The error in the "too rigid" model approaches (from below) a final value when the web depth approaches zero, due to the contribution of the extra portion of the web in the half thickness of the plate.

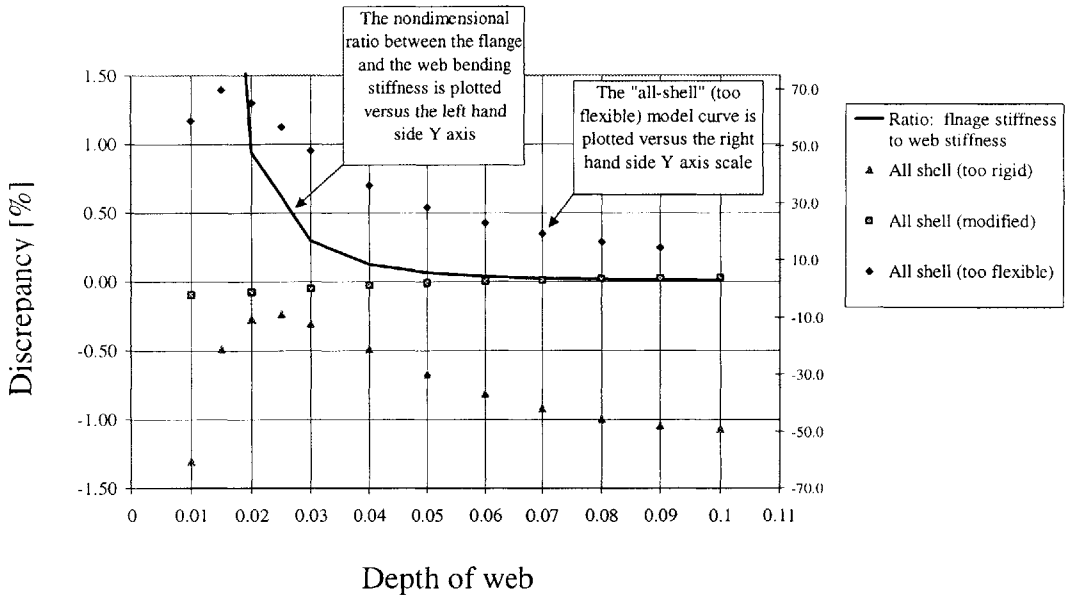

Figure 4-9: Cantilever beam with "T" cross-section – evaluation of the "all-shell" models tip displacement solution

- Cross-section definition – approach no. 2.

Another possible approach to tackle the problem is to define the distance between the midsurface of the flange and the bottom of the web as the value of the real height of the web – see Figure 4.8c. This approach leads to a too-flexible model (relative to the real structure) due to the reduction of the offset of the web, and as a result, reduction of the cross-sectional moment of inertia. This model has a substantial error compared to the exact solution: for the reference beam, the tip deflection has an error of 14% relative to the analytical solution.

- Cross-section definition – approach no. 2 – influence of the web's depth.

As for the "too rigid" model definition, the value of the discrepancy varies with the depth of the web, and *has a maximum value* (about 70%) *at the point where the bending stiffness of the flange and the web are equal* – see Figure 4-9. This is due to the relative influence of the incorrect location of the web on the overall bending stiffness of the cross section. When the bending stiffness of the flange is very large compared to the web, the contribution of the web to the overall stiffness is relatively small. Hence, the fact that the

web is misplaced has a minor importance. The same reasoning applies when the web stiffness is much larger than that of the flange: the cross section is mainly the web, so the relative location between the flange and the web has little importance. Once both the flange and the web make similar contributions, then the moment of inertia of the whole cross-section is affected in a dramatic way.

The maximum discrepancy between the "too flexible" model and the reference solution is smaller if the flange (which is kept fixed while the web's depth is varied) is larger. This is due to the fact that a deeper web is needed in order to match the stiffness of the flange – and hence the real distance between the mid-surface of the flange and the centroid of the web will be larger. As a result, the error involved with the misplacement of the web will be relatively smaller, since the ratio between the actual offset and the real offset value is smaller for this case. This phenomenon is demonstrated with the "T" cross-section no. 2, described in Figure 4-1b. This "T" cross-section has a thicker and wider flange, and a thinner web. Hence, the maximum discrepancy has a lower value (about 43%), and it is obtained for a deeper web – see Figure 4-10.

• Cross-section definition – approach no. 3.

In order to achieve a better representation of the cantilever beam using an all-shell element model, a third approach can be used. According to this approach, the depth of the web is defined such that the whole cross-section (web and flange) will have the same moment of inertia as the real cross section. The procedure to obtain the appropriate web depth is described below.

The moment of inertia of the real cross-section is given by the following expression:

$$I_{Real} = \frac{t_w h_w^{\,3}}{12} + t_w h_w d_w^{\,2} + \frac{b_f t_f^{\,3}}{12} + t_f b_f d_f^{\,2} \qquad (4.5)$$

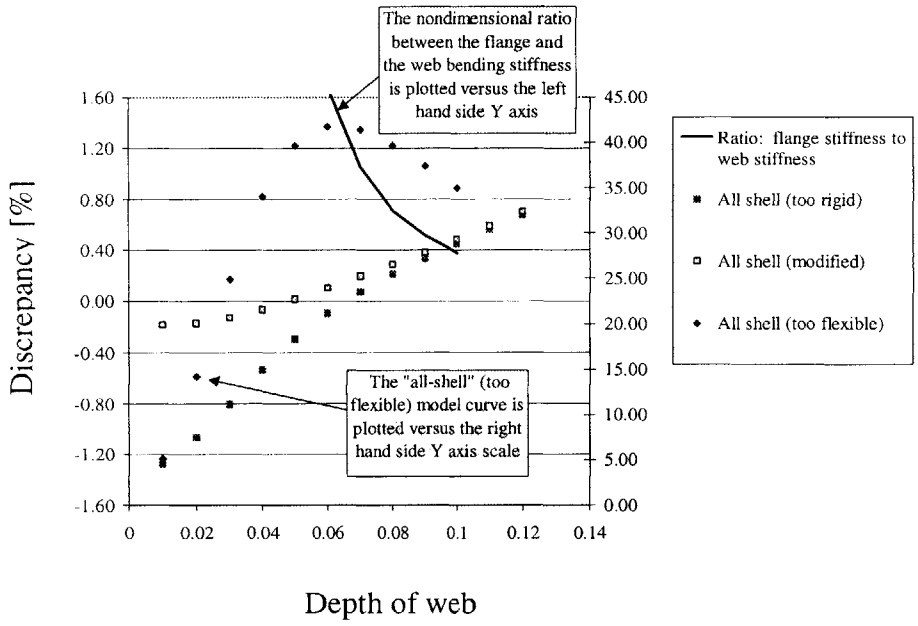

Figure 4-10: Cantilever beam with wide flange "T" cross-section – evaluation of the "all-shell" models tip displacement solution

The various terms are depicted in Figure 4-11a. The terms d_w and d_f are the distances from the cross-section neutral axis to the centroids of the web and the flange, respectively. These distances are given by the following expressions:

$$d_w = \frac{t_f b_f (h_w + \frac{t_f}{2}) + t_w \frac{h_w^{\,2}}{2}}{t_f b_f + h_w t_w} - \frac{h_w}{2} \tag{4.6}$$

$$d_f = h_w + \frac{t_f}{2} - \frac{t_f b_f (h_w + \frac{t_f}{2}) + t_w \frac{h_w^{\,2}}{2}}{t_f b_f + h_w t_w} \tag{4.7}$$

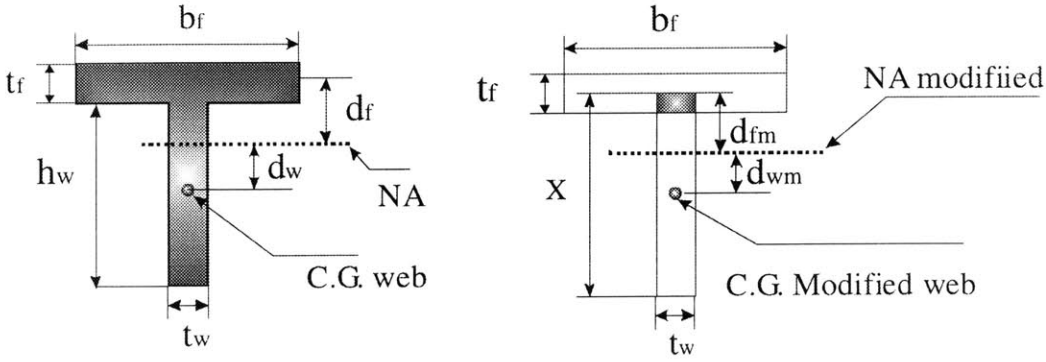

Real cross-section

4-11a

"All shell" model

modified cross-section

1-11b

Figure 4-11: Modified "all-shell" model – definition of cross-section

The cross-section of the modified all shell model is described in Figure 4-11b. The moment of inertia of this cross-section is given by:

$$I_{Modified} = \frac{t_w x^3}{12} + t_w x d_{wm}^{\ 2} + \frac{b_f t_f^{\ 3}}{12} + t_f b_f d_{fm}^{\ 2} \tag{4.8}$$

It should be noted that the term x is the depth of the modified web, which is to be calculated. The terms d_{fm} and d_{wm} are the distances from the neutral axis of the modified cross-section to the centroids of the flange and the modified web, respectively. They are given by:

$$d_{fm} = x - \frac{t_f b_f x + t_w \frac{x^2}{2}}{t_f b_f + x t_w} \tag{4.9}$$

$$d_{wm} = \frac{t_f b_f x + t_w \frac{x^2}{2}}{t_f b_f + x t_w} - \frac{x}{2} \tag{4.10}$$

Since we wish to define the modified cross-section such that it will have the same moment of inertia as the real cross section, we require that:

$$I_{Real} = I_{Modified} \tag{4.11}$$

By substituting (4.5), (4.6), (4.7), (4.8), (4.9) and (4.10) into (4.11), and dropping identical terms from both sides, we get:

$$\frac{t_w h_w^3}{12} + t_w h_w \left(\frac{t_f b_f (h_w + \frac{t_f}{2}) + t_w \frac{h_w^2}{2}}{t_f b_f + h_w t_w} - \frac{h_w}{2}\right)^2 + t_f b_f \left(h_w + \frac{t_f}{2} - \frac{t_f b_f (h_w + \frac{t_f}{2}) + t_w \frac{h_w^2}{2}}{t_f b_f + h_w t_w}\right)^2 =$$

$$= \frac{t_w x^3}{12} + t_w x \left(\frac{t_f b_f x + t_w \frac{x^2}{2}}{t_f b_f + x t_w} - \frac{x}{2}\right)^2 + t_f b_f \left(x - \frac{t_f b_f x + t_w \frac{x^2}{2}}{t_f b_f + x t_w}\right)^2 \tag{4.12}$$

Equation (4.12) can be simplified to:

$$x^3 \frac{t_w x + 4 t_f b_f}{t_f b_f + t_w x} = h_w \frac{h_w^3 t_w + 4 h_w^2 t_f b_f + 6 t_f^2 b_f h_w + 3 t_f^3 b_f}{t_f b_f + t_w h_w} \tag{4.13}$$

The value of x, the modified depth of the web, can be obtained by an iterative solution.

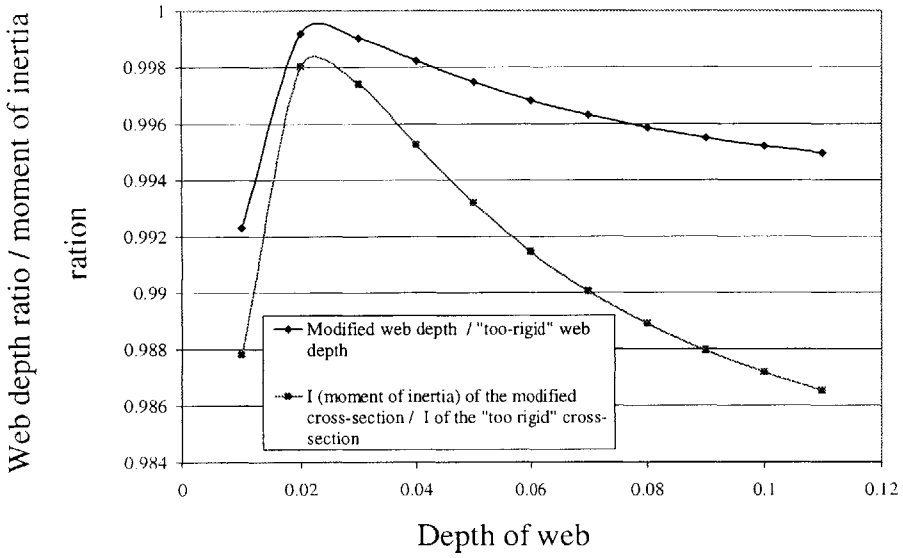

Figure 4-12: Modified web depth and moment of inertia.

Figure 4-12 describes the ratio between the modified web depth (x) to the real web depth (h_w). It can be noted that the depth of the modified web is very close to the depth of the real web. This means that the too-rigid all-shell model is only "slightly too rigid", as demonstrated in Figure 4-12 by the ratio of the moments of inertia.

The modified all shell model, which uses the modified web depth, yields displacements that are very close to the three-dimensional model solution. The displacement solutions for the various web depths, as obtained by the modified all-shell model, are given in Figure 4-9 for the reference beam, and in Figure 4-10 for the wide flange "T" cross-section.

4.3.4.2 Predicted stresses

Figure 4-13 gives the bending stresses, as obtained by the various "all shell" models. It is noted that the too-flexible shell model yields higher stresses than the three-dimensional model or the analytical solution - about 9.8% higher than the three-dimensional solution near the fixed end of the beam. The too-rigid shell model solutions are about 1% smaller

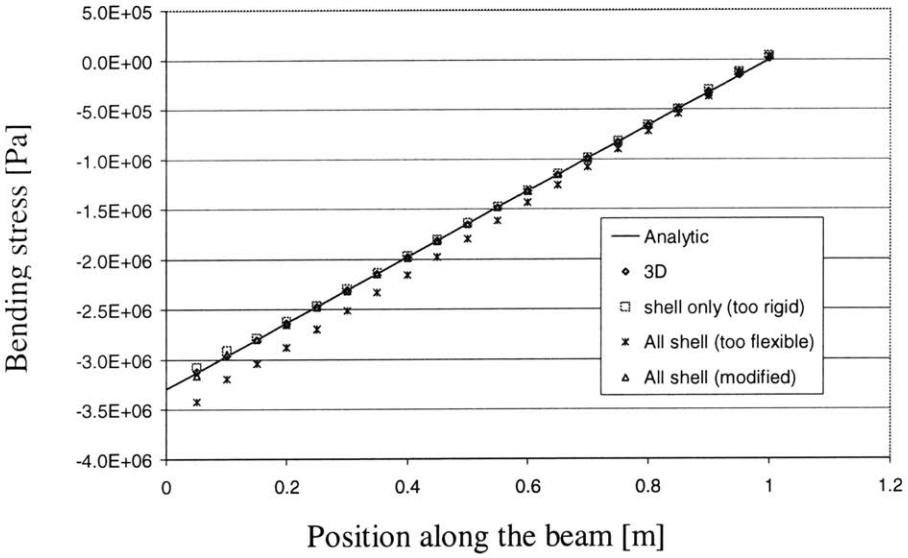

Figure 4-13: "All-shell" model – bending stresses

than the three-dimensional solution, and the modified all-shell model error is below 0.5%. The shear stresses due to bending are well predicted by the all-shell models, as describes in Figure 4-7.

4.3.5 Over-all comparison

The comparison of the displacement solution of the three-dimensional model to the solutions obtained with the other models, as a function of the depth of the web, is summarized in Figure 4-14.

It can be seen that the modified "all shell" model solution is the closest to the three-dimensional model solution. The original "Hermitian model" solution error increases with the web depth since the distance between the mid-surface of the flange and the neutral axis of the cross-section is increasing, as the web becomes deeper.

The modified "Hermitian model", the "Iso-beam model" and the modified all-shell model solutions are within ±0.25% of the three-dimensional model solution in the investigated range of cross-sections.

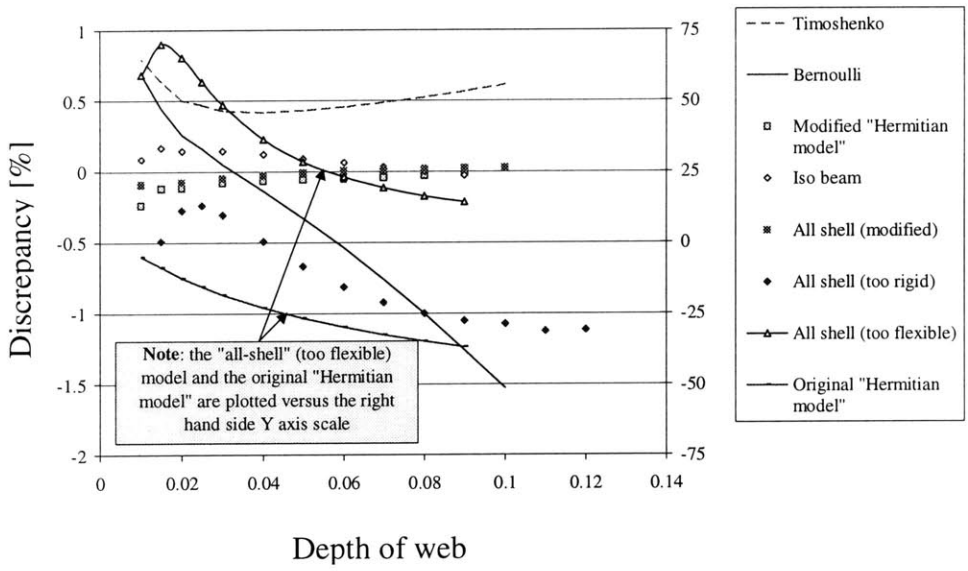

Figure 4-14: Cantilever "T" beam – comparison of all models to the 3D model

4.4 Conclusions reached from the analyses

The results obtained from the demonstrating problems lead to several conclusions, regarding the modeling of a stiffened plate structure.

- Modeling a stiffened plate structure using a combination of Hermitian beam and shell elements.

In a similar way to the modeling of a "T" cross-section, a stiffened plate model that is constructed from Hermitian beam and shell elements will be too rigid, if the value of the offset is not properly adjusted.

It should be noted, though, that when modeling a stiffened plate, the error described above would be less significant, since the neutral surface of the stiffened plate is located close to the plate. However, one should be aware of the existence of the error, which may result in smaller deflections and stresses relative to those obtained by the three-dimensional model.

- Modeling a stiffened plate using Hermitian or iso-beam elements, and shell elements.

The results obtained from the analysis of cantilever beams demonstrated that models constructed from Hermitian beam or iso-beam elements with shell elements cannot predict correctly the flow of the shear stresses from the flange to the web. This is due to the lack of shear compatibility between the plate and beam elements.

- Modeling a stiffened plate using only shell elements.

Construction of a model with intersecting shells, which are defined by their mid-surfaces, will yield an error due to the overlapping zones – as demonstrated above. If the "too flexible" approach is used, the displacement solution will be substantially in error. The maximum error occurs when the bending stiffness of the stiffener is equal to the bending stiffness of the effective breadth of the plate. The effect on a stiffened plate structure is described in Section 5.

5 Analyses of stiffened plate

5.1 Introduction

The main goal of the thesis research was to investigate different methods to model stiffened plate structures, and to gain insight into the modeling capabilities of each method. The study of the modeling capabilities, as described in the last chapter, contributed to the understanding of the mechanics of each modeling method, and the ability to make several modifications in order to improve their performances. The modifications were proved to be efficient for the cantilever beam geometry, and herein they are examined for a stiffened plate structure.

The stiffened plate is described in Figure 5-1. The structure consists of a plate and two sets of orthogonal stiffeners and is subjected to a uniform pressure of 9800 [Pa], the equivalence of 1 [m] height of water column. Two boundary condition cases were examined: clamped and simply supported edges.

Four types of models were constructed and solved using ADINA (see Figure 5-2):

1. "Hermitian beam" model: constructed from Hermitian beam and 4-node shell elements. The offset of the Hermitian beam elements was defined using two approaches (see discussion on Hermitian beam definition approaches in Section 4.3.2): "original" and "modified" offset definition.
2. "Iso-beam" model: constructed from isoparametric beam and 8-node shell elements.
3. "All-shell" model: constructed from 8-node shell elements. Three "all-shell" models were studied (see definitions in Section 4.3.4): the "too flexible" model, the "too rigid" model and the "modified" model.
4. Three-dimensional model: constructed from 27-node three-dimensional elements.

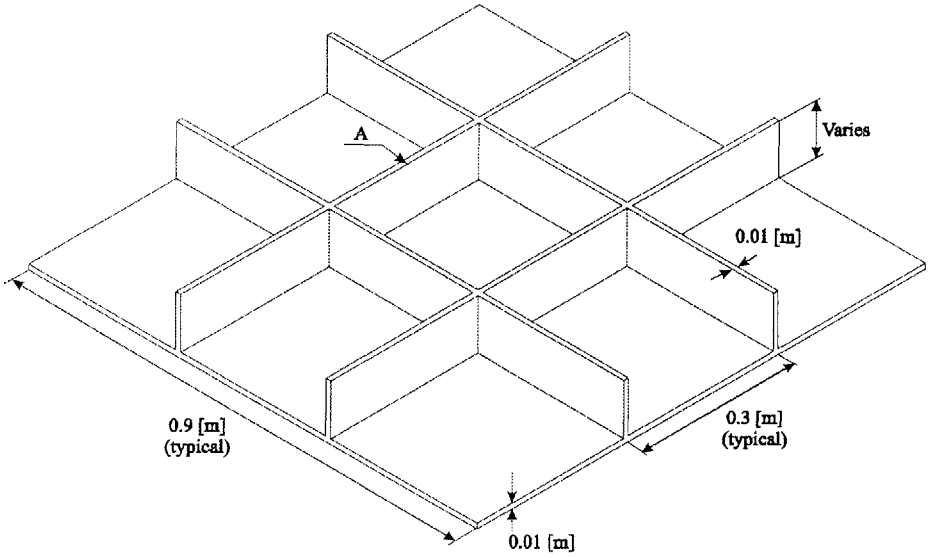

Figure 5-1: Geometry of the stiffened plate under investigation.

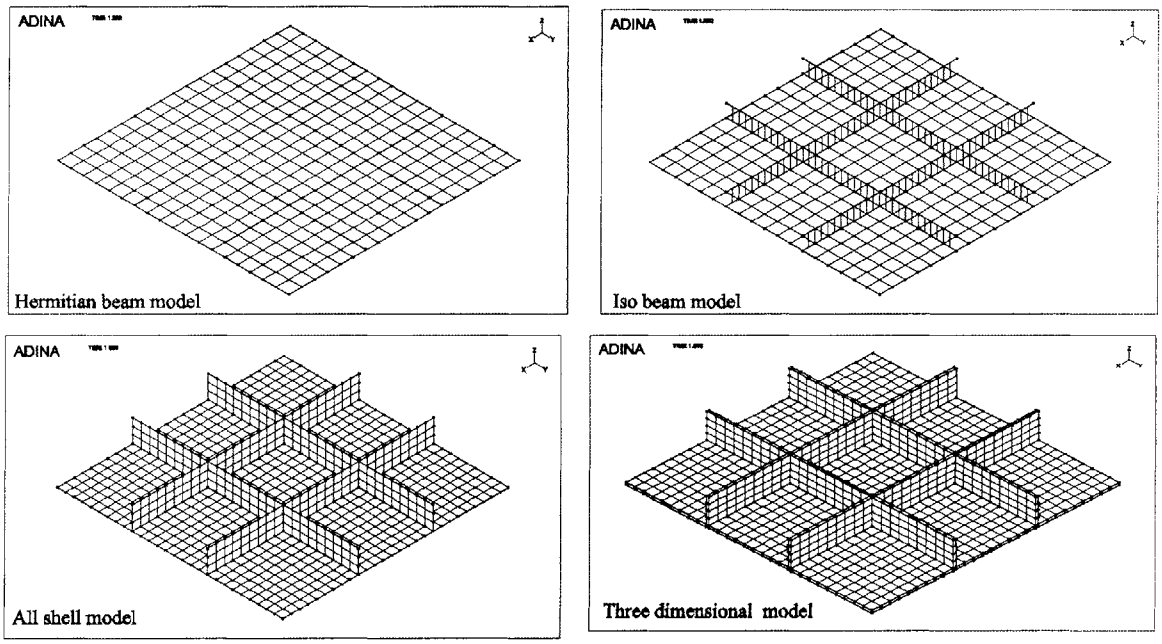

Figure 5-2: Finite element models of stiffened plate.

As already discussed in Chapter 4, the solution of a three-dimensional model provides the best prediction of the response of the real structure, since the model does not include pre-defined assumptions about the mechanics of the structure. Our objective is to evaluate the performances of the simplified finite element models (models number 1 to 3 from the list above) by comparing their solutions to the solution of the three-dimensional model. Doing so allows us to evaluate the predicted solutions of displacements and stresses. The comparison was conducted for different depths of stiffeners, in order to generalize the conclusions derived from the investigation.

We begin with the derivation of an approximate analytical solution to the physical problem. This solution served to assess the order of magnitude of the stiffened plate response, as obtained by the finite element model solutions.

5.2 Analytical solution

The analytical solution was obtained by solving the Huber equation for orthotropic plates. In the following we describe the analytical solution for the case of simply supported edges, where the different dimensions of the stiffened plate structure are as given in Figure 5-1, with stiffeners' depth of 0.1 [m].

The Huber equation for an orthotropic plate under distributed load (pressure) P is:

$$D_x \frac{\partial^4 w}{\partial x^4} + 2H \frac{\partial^4 w}{\partial^2 x \partial^2 y} + D_y \frac{\partial^4 w}{\partial y^4} = P(x, y) \tag{5-1}$$

where

$$D_x = \frac{E I_x}{b_1}$$

$$D_y = \frac{E I_y}{a_1}$$

$$D_{xy} = \frac{G}{3}\left(\frac{h_1 d_1^{\,3}}{a_1} + \frac{h_2 d_2^{\,3}}{b_1}\right)$$
$$G = \frac{E}{2(1+\nu)} \tag{5-2}$$
$$H = \frac{Et^3}{12(1-\nu^2)} + D_{xy}$$

The definition of h_1, h_2, a_1, b_1, d_1, d_2 and t are given in Figure 5-3, for a general case of stiffened plate structure. For the stiffened plate structure discussed here, we have $h_1=h_2=0.1$ [m], $a_1=b_1=0.29$ [m] and $d_1=d_2=0.01$ [m]. I_x and I_y are the moments of inertia of the combined cross section (plate and stiffeners together).

The Huber equation has a general solution of the form:

$$W(x,y) = \sum_{m=1}^{\infty}\sum_{n=1}^{\infty} B_{mn} \sin\left(\frac{m\pi y}{a}\right)\sin\left(\frac{n\pi x}{b}\right) \tag{5-3}$$

We can express a uniform pressure P_0 over the area of the plate (a in length, b in width) by the following series expression:

$$P = \sum_{m=1}^{\infty}\sum_{n=1}^{\infty} \frac{16P_0}{\pi^2 mn}\sin\left(\frac{m\pi\ y}{a}\right)\sin\left(\frac{n\pi\, x}{b}\right) \tag{5-4}$$

By substituting the general solution for W(x,y) in (5-3) and the expression for P_0 in (5-4), into (5-1), and by dropping common terms, we get:

$$B_{mn}\left(\frac{\pi^4 m^4}{a^4} D_y + \frac{\pi^2 m^2 n^2}{a^2 b^2} 2H + \frac{\pi^4 n^4}{b^4} D_x\right) = \frac{16P_0}{\pi^2 mn} \tag{5-5}$$

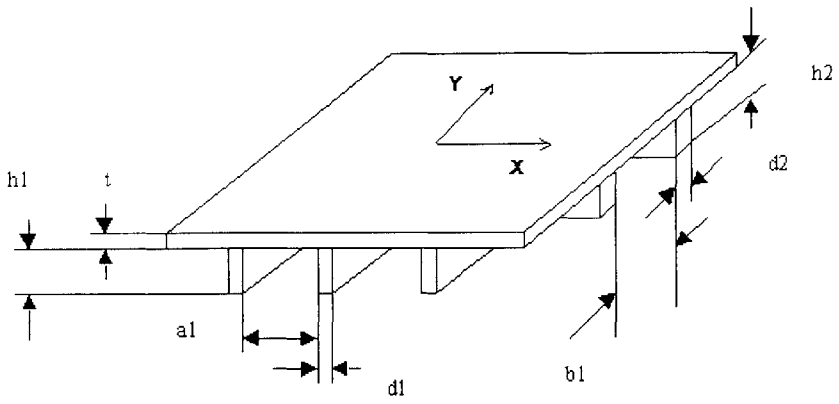

Figure 5-3: Definitions of the terms in the Huber equation.

and so the coefficients for the general solution in (5-2) are:

$$B_{mn} = \frac{16P_0}{\pi^2 mn} \frac{1}{\left(\frac{\pi^4 m^4}{a^4} D_y + \frac{\pi^4 m^2 n^2}{a^2 b^2} 2H + \frac{\pi^4 n^4}{b^4} D_x\right)} \tag{5-6}$$

Using MATHCAD, the different coefficients were calculated (in principle, the coefficients should be calculated with n=m=1..∞, but a sufficient accuracy can be obtained with n=m=1..100), and the displacements W(x,y) were derived. Figure 5-4 describes the displacements of the structure, as obtained from the solution of the Huber equation. The maximum deflection (in the center of the plate, as can be expected) is $1.266*10^{-5}$ [m].

As discussed later, the three-dimensional model solution for the same physical problem yielded a maximum deflection of $2.941*10^{-5}$ [m], which has the same order of magnitude as the result obtained by the analytical solution. Obviously, once we find that

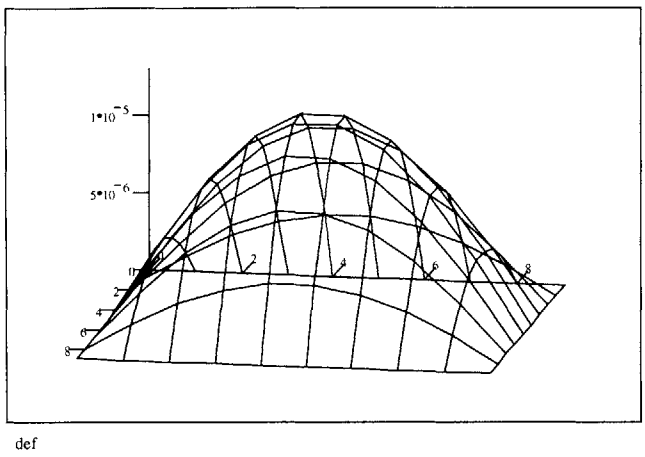

Figure 5-4: Solution of the Huber equation.

the comprehensive finite element solution and the analytical solution are of the same order of magnitude, we should note that the finite element solution is more accurate (closer to reality), since it does not include the assumptions and approximations involved within the analytical solution.

5.3 Solutions of finite element models

The response of the stiffened plate described in Figure 5-1 was investigated for two boundary condition cases: clamped and simply supported edges. For each boundary condition case, a series of models of stiffened plates was constructed and solved. Each model was defined with different depth of stiffeners, which was varied from 0.1 [m] to 0.01 [m]. In the following, we focus on the evaluation of the displacement and stress solutions of the various models.

5.3.1 Clamped edges boundary condition.

The clamped boundary condition is modeled by fixing all the degrees of freedom at the outer edges of the plate and stiffeners: three degrees of freedom in the three-dimensional

model (three translations) and six degrees of freedom for all other models (three translations and three rotations).

• Predicted displacements

The maximum displacement of a stiffened plate structure subjected to a uniform pressure load is naturally obtained in the center of the plate. Figure 5-5 describes the displacement in this location as obtained by the various models, for different depths of stiffeners. It can be noticed that all the models yielded similar results, except the "too-flexible" all-shell model, which yielded substantially larger (and erroneous) displacements.

We evaluate the displacement solutions of the various models by comparison to the three-dimensional solution, as described in Figure 5-6. From this comparison a significant result arises: the modified all-shell model yields solutions that differ from the three-dimensional solution by up to 6.21%, a discrepancy which is larger (in absolute values) than the discrepancies of the iso-beam and the modified Hermitian models. This result might be thought of as surprising if we recall that for the cantilever beam case, that was covered in Chapter 4, the modified all-shell model yielded almost the same results as the three-dimensional model (within 0.09%). Furthermore, the "too-rigid" all-shell model, which can be expected to yield *smaller* displacements than the three-dimensional model, is found to be more flexible by up to 6.13%.

As can be noticed, the modified and the "too-rigid" all-shell models yielded almost the same solutions, which implies that the modified and "too-rigid" stiffener depths are very close (see definitions of modified and "too rigid" depth values in Figure 4-8). This is due to the nature of the modification method, which involves the width of the flange (or in the case of a stiffened plate, the width of the plate that is taken as the flange). As the width increases, the modified stiffener depth approaches the "too-rigid" value since the extra portion of the stiffener inside the plate has negligible contribution to the overall

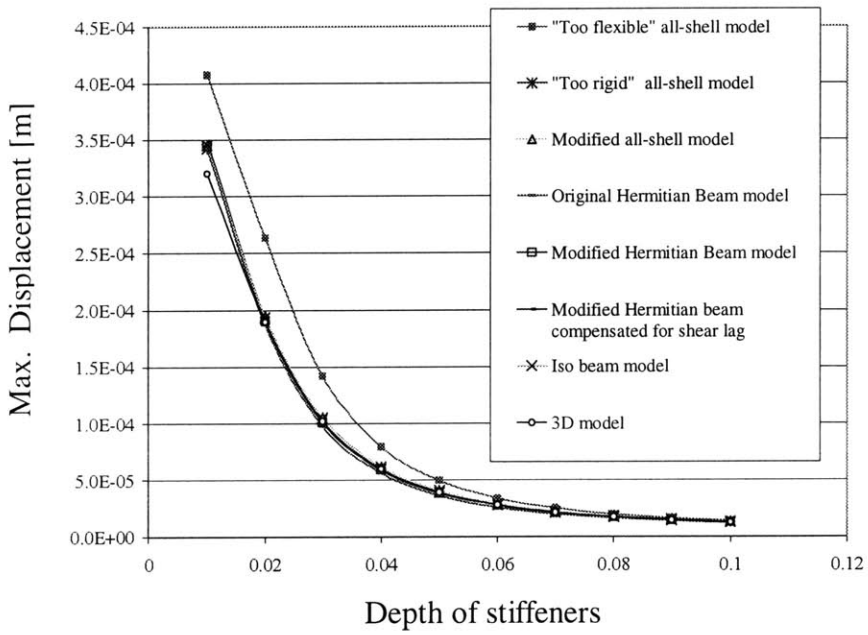

Figure 5-5: Stiffened plate with clamped edges – maximum displacement as function of the depth of the stiffeners.

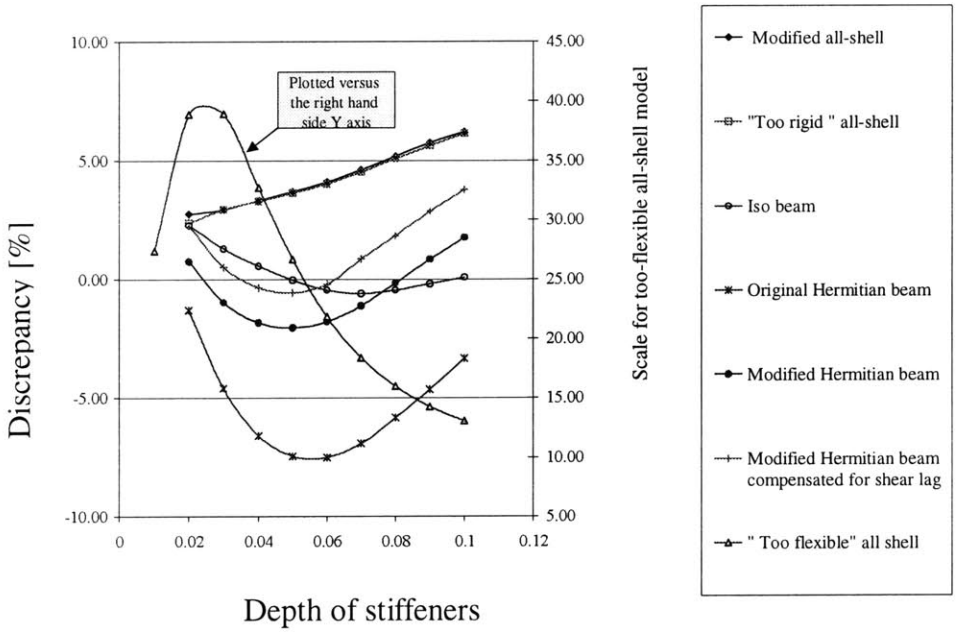

Figure 5-6: Discrepancy of the maximum displacement as predicted by the various models relative to the three-dimensional model solution.

bending stiffness, and hence the original all-shell model is not altered in a significant way.

The discrepancy between the all-shell model displacement solutions and the three-dimensional solution, is mainly due to the way in which the thickness of the plate and stiffeners is modeled. In the three-dimensional model the plate and stiffeners are modeled in a natural and accurate way that corresponds to the real three-dimensional geometry of the structure. In the all-shell models we represent the plate and the stiffeners by flat two-dimensional shell elements, where the physical thickness of the real structure is defined separately from the definition of the geometry itself. This thickness definition is used in the element stiffness matrix calculation (see Chapter 3), and hence the mechanics of the real structure is, in general, represented accurately. The problem arises when we have intersections of shells: due to the two-dimensional nature of the shell elements they cannot predict three-dimensional effects that exist in nature.

In the studied stiffened plate structure this phenomenon appears in the intersection between the stiffeners, and the intersection between the stiffeners and the plate. A two-dimensional all-shell model cannot represent these intersections correctly, as demonstrated in Figure 5-7(a), since it cannot predict the influence of the thickness of the stiffener on the deformed shape of the plate (or the thickness of one stiffener on the deformed shape of another stiffener). This influence is well predicted by the three-dimensional model as shown in Figure 5-7(b).

As a result of the lack of ability to predict three-dimensional effects, the all-shell models are too flexible and yield larger displacements than the three-dimensional model as shown in Figure 5-6. In order to further assess the effect of this phenomenon, a new modified all-shell model was defined: in this model rigid links were used to link the nodes of the plate under the stiffeners, in order to imitate the effect of the stiffeners' thickness. This new modified all-shell model yielded a displacement solution that is very close to the three-dimensional solution: for stiffener depth of 0.1 [m] the discrepancy of the maximum displacement was 0.4%. We can conclude that the way by which the

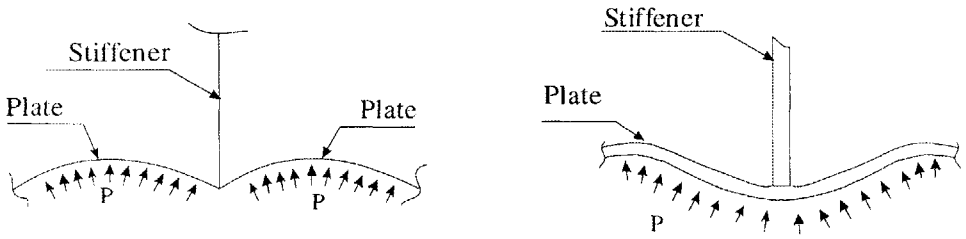

(a) All shell model (b) Three-dimensional model

Figure 5-7: Intersection between plate and stiffener.

thickness of the stiffeners is modeled has a substantial effect on the displacements solution.

All of the other models (iso-beam model, original and modified Hermitian beam model) contain the same problem, since they all use one- and two-dimensional elements, which cannot predict three-dimensional effects. Fortunately, the extra-flexibility introduced by this phenomenon is balanced by the extra-rigidity already existing in the Hermitian beam and iso-beam models, extra rigidity that is caused by the assumptions within the models. This balancing of the two influences leads to relatively good results of the modified Hermitian beam and iso-beam models, as shown in Figure 5-6.

In the iso-beam model, the extra rigidity is introduced by the rigid links that connect the beams to the plate (see Figure 5-2). The outcome of a rigid link is that one node (the "slave" node, in this case a given node along the beam) is constrained to translate so that the distance between it and another node (the "master" node, in this case the corresponding node in the plate) is constant, and further constrained to rotate with the same rotation as the master node. In the real physical problem, these constraints on the displacements of the material particles do not exist, of course, and hence extra-rigidity is introduced into the iso-beam model.

In the Hermitian beam models (original and modified) extra-rigidity is introduced by the fact that the *shear-lag* effect cannot be predicted. Let us discuss briefly the essence of the shear-lag phenomenon.

Simple beam theory assumes that plane cross-sections remain plane, and that therefore the bending stress is directly proportional to the distance from the neutral axis. Thus in any flange-and-web type of beam the predicted stress is constant across the flange. However, in reality, the bending loads applied on the beam deflect the web to some radius of curvature, thus inducing large strain in the flange. Since it carries large strain, and hence large stress, the flange makes the significant contribution to the bending stiffness. It is important to note that this large strain comes initially from the web and only reaches the flange by shear. This is demonstrated in Figure 5-8, which shows a wide flange "T" beam loaded with a vertical force. The web deflects such that the upper and lower edges of the web are elongated and shortened. At the upper edge the elongated web pulls the plating with it, resulting into in-plane shear forces, which sets up shear stresses in the flange. The bending and shear stresses cause stretching and in-plane distortion of the flange. In the figure an element is shown before and after this distortion: the shear distortion is such that the outer edge of the element does not have to stretch as much as the inner edge. That is, the longitudinal strain is less at the outer edge and therefore so is the longitudinal stress. This same phenomenon will occur at each element, from the centerline to the edges, although it will diminish steadily and disappear at the edges because the shear stress diminishes to zero. The overall result is that the flange undergoes in-plane longitudinal distortion and therefore *plane cross-sections do not remain plane.* This distortion is commonly referred to as "warping" of the cross section. The most significant aspect of the shear distortion is that the outer portion of the flange carries less bending stress, and is therefore less effective than the inner portion. That is, due to shear effects, the bending stress remote from a web "lags behind" the stress near the web, and hence the phenomenon is termed "shear lag" effect. Shear lag is of importance in beams having very wide flanges and shallow webs, or in stiffened plates with wide spacing between the stiffeners.

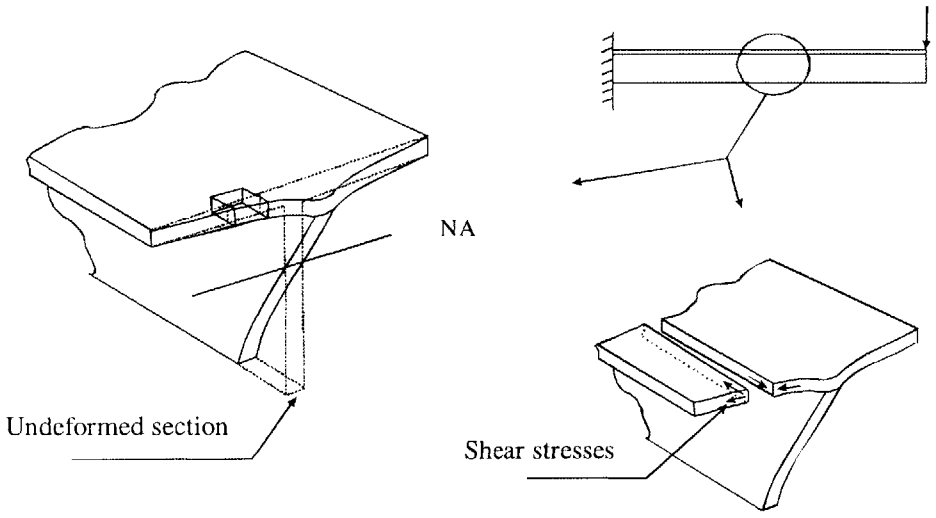

Figure 5-8: Shear lag in a wide flange "T" beam.

As mentioned above, the shear lag effect cannot be predicted accurately by the Hermitian beam model. This is a consequence of the way in which the model is constructed: the Hermitian beam elements are defined in the plane of the plate (see Figure 5-2), and hence the transmission of the longitudinal strains of the stiffeners to the plate by shear forces is not predicted. As a result, the whole breadth of the plate is effective in bending and extra-rigidity is introduced to the Hermitian beam model.

As described in Section 4.3.2, the *modified* Hermitian beam is defined by adjusting the offset of the stiffener from the flange (or the offset of the web from the flange, in the case of the "T" beam model) such that the resulting combined section will have the same moment of inertia as the section of the real structure. Since the calculation of the adjusted offset involves the breadth of the plate, we can use an effective plate breadth in order to indirectly include the shear lag phenomenon in the model. The effective breadth of the plate for different types of structures and loadings cases may be found in various references (see [10] for example). The effective breadth of the stiffened plate analyzed herein, for the case of clamped edges, is 58% of the stiffeners spacing.

By applying this approach to the analyzed stiffened plate, a new series of Hermitian beam models was constructed and solved. The displacement solutions obtained by these models (referred to as "modified Hermitian beam model, compensated for shear lag") are described in Figure 5-6. It can be noticed that by involving the shear lag

phenomenon in the models we obtain larger displacements, as expected. One should keep in mind that this approach only roughly approximates the shear lag phenomenon, and hence will not yield an accurate prediction of the effect obtained via three-dimensional model.

• Predicted stresses.

From the comparison of the various models on the basis of maximum deflection, we can conclude that the "too-flexible" all-shell model can not be considered as an appropriate model for the stiffened plate structure. Hence, the stress investigation was limited to the original and modified Hermitian beam models, iso-beam model, and the "too-rigid" and modified all shell models.

The bending stresses in the mid-span of the stiffeners (point A in figure 5-1) were investigated. Although the maximum stresses in a clamped stiffened plate subjected to uniform pressure are obtained at the clamped edges, the investigation of the stresses was focused on the mid-span of the stiffeners in order to isolate the influence of the singularities introduced by the sharp corners at the clamped edges.

Since the natural axes are located between the plate and the mid-depth of the stiffeners, the maximum bending stresses in the stiffeners are obtained in the fibers which are most remote from the plate. Due to the symmetry of the structure and loading, the same bending stress was obtained in all of the stiffeners. Figure 5-9 gives the stresses predicted by the various models, as a function of the depth of the stiffeners. It can be noticed that the three-dimensional model, all shell models and the iso-beam model predicted very similar results.

Figure 5-10 shows the discrepancies in bending stresses between the three-dimensional model and the rest of the models. As expected, the prediction of higher

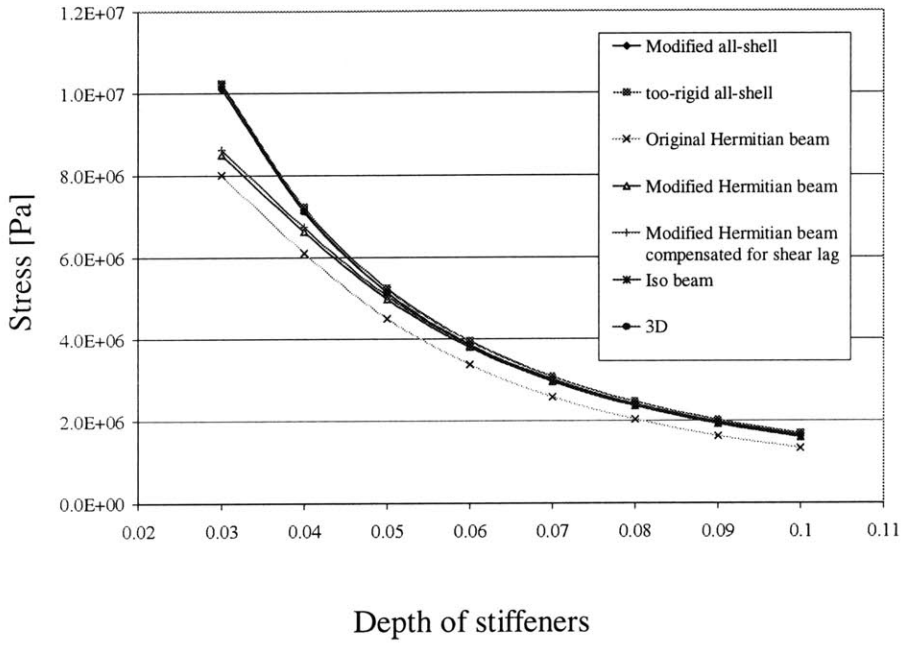

Figure 5-9: Stiffened plate with clamped edges – bending stresses in the stiffeners.

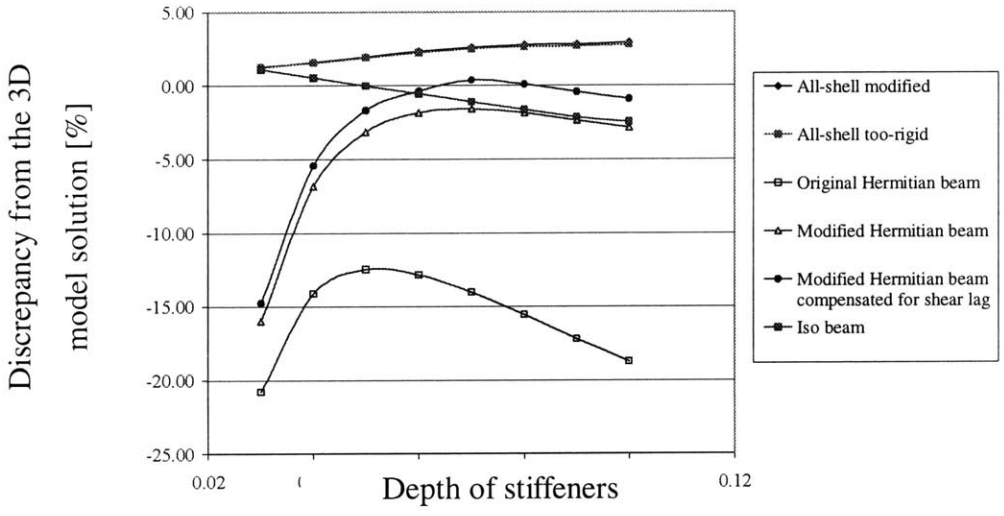

Figure 5-10: Stiffened plate with clamped edges – evaluation of bending stresses.

displacements by the all-shell models (relative to the three-dimensional model) led to higher stress prediction, up to a maximum discrepancy of 2.9% for stiffener height of 0.1[m].

The iso-beam model yielded higher stresses than the three-dimensional model for depth of stiffeners smaller than 0.05 [m], and lower stresses above this stiffener depth. This trend of the stress discrepancy resembles the trend of the displacement discrepancy of this model.

The original Hermitian beam model yielded smaller stresses than the three-dimensional model, with a maximum discrepancy of about –20%. It can be noted that the trend of the stress discrepancy is inverse to the trend of the displacement discrepancy: for depth of stiffeners of about 0.05 [m] the displacement discrepancy is the maximum, while the stress discrepancy is the least. This is due to the way in which the load is distributed between the stiffeners and the plate: when the stiffeners are modeled as too-stiff by the Hermitian beam model, the displacements are smaller but the relative percentage of the load carried by the stiffeners is larger, and so the predicted stresses are higher.

The modified Hermitian beam yielded better results than the original Hermitian beam model, with a discrepancy (relative to the three-dimensional model) of about –5% for depth of stiffeners of 0.05[m] and above. A further improvement was obtained by compensating the Hermitian beam model for shear lag in the plate. These results demonstrate the effectiveness of the modification process, when modeling stiffened plate structures with Hermitian beam elements.

5.3.2 Simply-supported boundary conditions

For the all-shell, iso-beam and Hermitian beam models, the simply supported boundary condition was applied by fixing only the translation degrees of freedom (and

enabling the rotations) at the edges of the plate. In the three-dimensional model, where only translation degrees of freedom exist, the nodes at the mid-thickness of the plate were fixed, such that rotations about the mid-thickness are enabled.

• Predicted displacements.

Figure 5-11 gives the displacements at the center of the plate, as obtained by the various models, for different depths of stiffeners. The figure also includes the solution of the approximated analytical solution presented in the beginning of the chapter. The discrepancies between the two- and three- dimensional model solutions are shown in Figure 5-12. The major observations made in the case of the clamped edges boundary condition repeat here: the modified and "too-rigid" all-shell models yield larger displacements than the three-dimensional model, with a maximum discrepancy of about 2.46% for depth of stiffeners of 0.1[m].

It can be noticed from Figure 5-12 that the maximum discrepancy of the "too-flexible" all-shell model is obtained for depth of stiffeners of 0.03 [m], while the maximum discrepancy of the same model with clamped edges boundary condition is obtained for depth of stiffeners slightly above 0.02 [m] (see Figure 5-6). The disparity is driven by the shear lag phenomenon which is well predicted by the all-shell models. The effective breadth of the plate depends on the distance between points of zero bending moment, which governs the radius of curvature of the deformed structure. Since in the clamped edges case the distance between points of zero bending moment is smaller, the effective breadth of the plate is smaller: 58% of the spacing between the stiffeners, compared with 71% in the simply supported case.

Since the maximum error of the "too-flexible" all-shell model is obtained when the bending stiffness of one stiffener is equal to the stiffness of the effective breadth of the plate, the difference in effective plate breadth leads to different depths of stiffeners for which a maximum discrepancy is obtained.

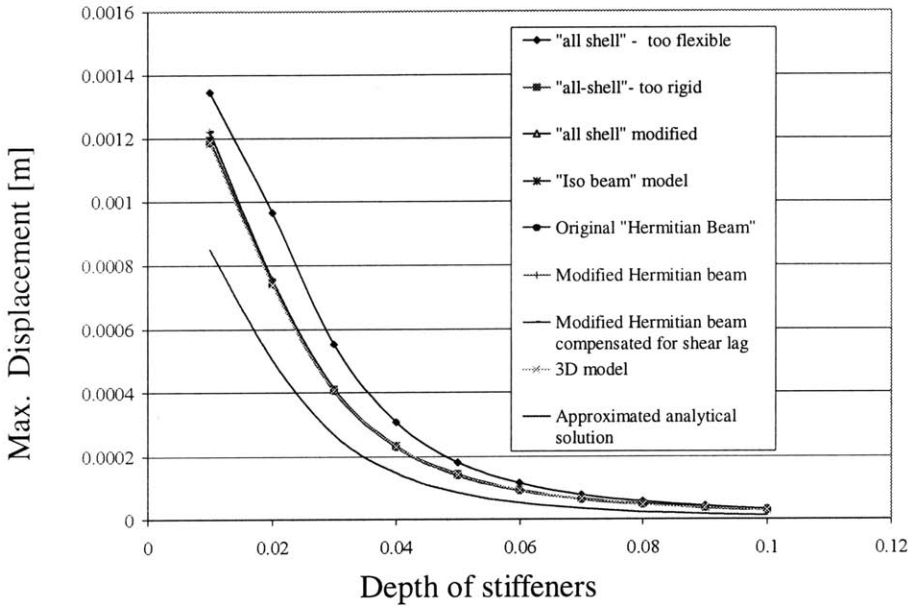

Figure 5-11: Stiffened plate with simply supported edges – maximum displacement as function of the depth of the stiffeners.

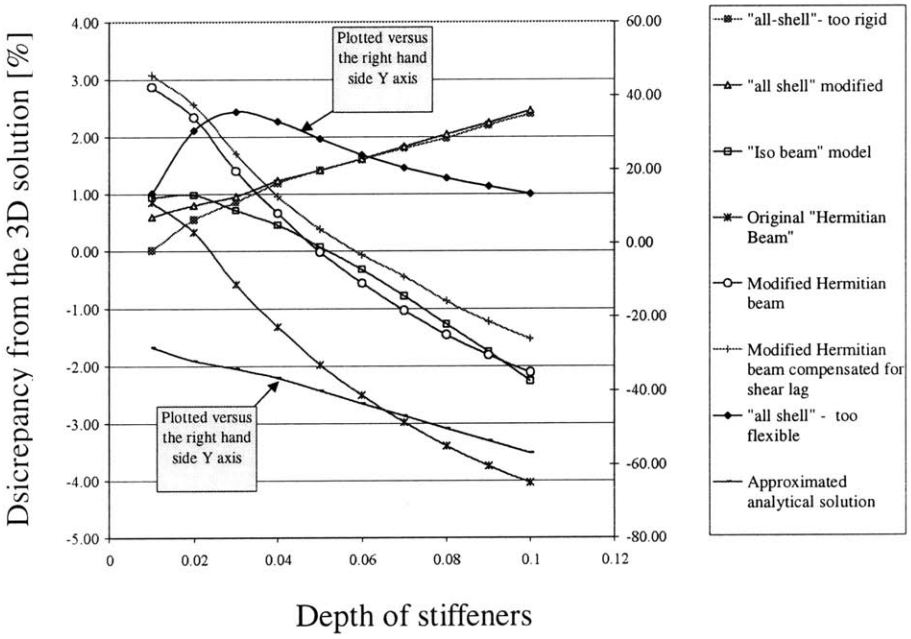

Figure 5-12: Stiffened plate with simply supported edges – discrepancy of displacement solutions from the 3D model solution

The approximate analytical displacement solution, obtained by the equivalent orthotropic plate method, yields considerably smaller displacements than the three-dimensional model. Even tough, the approximated analytical solution, due to its simplicity, can be easily used to verify the order of magnitude of a given finite element solution.

- Predicted stresses.

As for the clamped edges case, the bending stresses in the mid-span of the stiffeners were investigated. Figure 5-13 gives the stresses obtained by the various models while Figure 5-14 shows the discrepancy of the various stresses solutions from the three-dimensional solution. It can be noticed that the stress-discrepancy curves of the Hermitian beam models have an inverse trend to that seen in the displacement-discrepancy of the same models, as shown in Figure 5-12. The same phenomenon was observed and discussed in the case of the clamped edges boundary condition case.

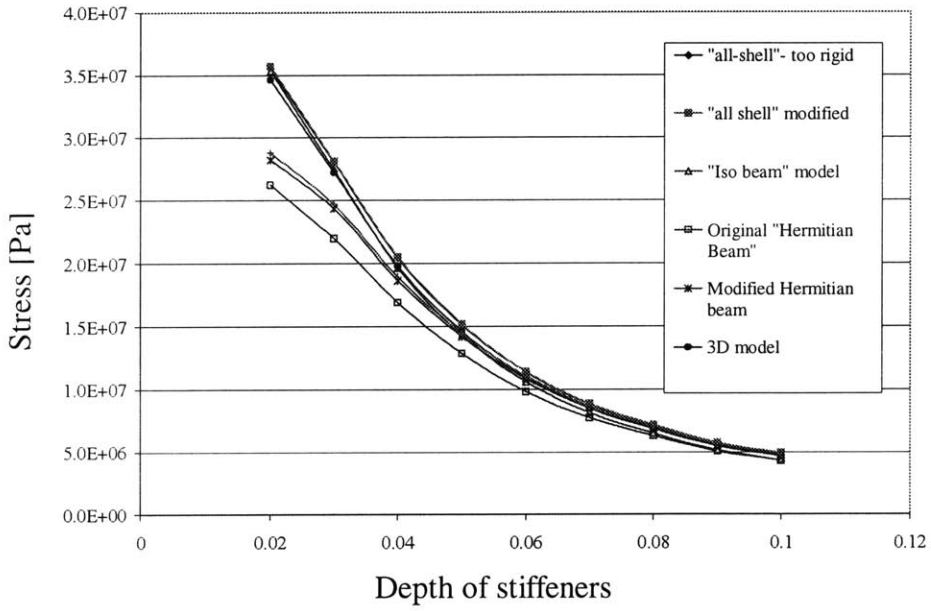

Figure 5-13: Stiffened plate with simply supported edges – bending stresses in the stiffeners

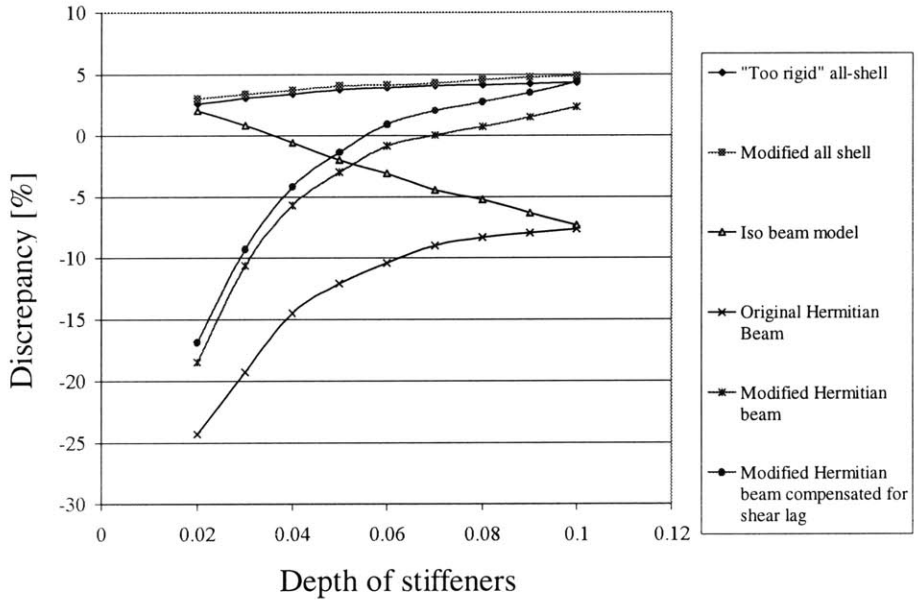

Figure 5-14: Stiffened plate with simply supported edges – discrepancy of bending stresses solutions from the 3D model solutio

6 Concluding remarks

We have described several ways to model stiffened plate structures using the finite element method, and discussed in detail the assumptions involved with each finite element model.

The modeling capabilities of the various elements were investigated thoroughly by constructing and solving finite element models of a simple "T" beam structure. In particular, we examined the influence of the depth of the web on the performances of the different modeling methods. Using the knowledge gained from this investigation, it was possible to perform several modifications to the original modeling methods, in order to improve their performances. These improved modeling methods were shown to yield enhanced displacement and stress predictions.

We have shown that the solution of a stiffened plate model that uses a combination of Hermitian beam and shell elements predicts significantly smaller deflections and stresses than those obtained by the corresponding three-dimensional model. We have offered a modification to this model, based on the adjustment of the way in which the eccentricity of the stiffeners is defined. This modified modeling method was shown to yield good results when used for modeling stiffened plate structures, subjected to different boundary conditions.

We have also shown that a stiffened plate model that uses Hermitian beam elements to model the stiffeners cannot predict accurately the shear lag phenomenon. This is a consequence of the position of the Hermitian beam elements in the model: they are placed in the plane of the plate, and hence the local transmission of the axial strain from the edge of the stiffeners to the plate (the essence of the shear lag phenomenon) can not be predicted accurately. We have offered further modification to the Hermitian beam model, in order to accommodate the influence of the shear lag phenomena.

Using shell elements to model the stiffeners, as well as the plate, is known to yield a good replica of the physical problem. We investigated the influence of the depth of the stiffeners on the performances of these models, and concluded that the intuitive approaches to model the depth of the stiffeners may result in considerable errors in the predictions of the displacements and stresses. Maximum errors are obtained when the bending stiffness of a single stiffener is equal to the bending stiffness of the effective plate to which it is attached. We have offered a modification to this modeling method, based on the adjustment of the definition of the stiffeners' depth. This modified depth allows for the inherent inaccuracy present in the modeling of the plate and stiffeners intersections (or web and flange intersection in case of a beam) using the shell elements.

We have shown that finite element models that use two-dimensional elements, such as shell elements, cannot predict the effect of the thickness of the stiffeners on the deformed shape of the plate, and hence they predict larger displacements than the three-dimensional element model. We have demonstrated that the influence of the stiffener thickness can be introduced into the shell element model by imposing rigid links along the intersections between the plate and the stiffeners. However, this process requires a very fine mesh and hence is not practical for large finite element models.

It is important to note that this research included only *static linear* structural finite element analysis for beam and stiffened plate structures. Hence, we can recommend the use of the modified modeling methods discussed above only when static linear analysis is considered. Therefore, it is recommended that future research on these modeling methods for stiffened plate structures will examine their validity for nonlinear analyses (large displacements, buckling) and dynamic (transient) analyses.

As a summary, it should be mentioned that all of the modeling methods discussed in this thesis are adequate for the analyses of stiffened plates. The employment of the modifications suggested above to the various modeling methods will yield more accurate solutions but will also require more engineering time. The decision whether to apply these modifications should be made according to the required accuracy of the solution,

depending on the physical problem and the analyst judgment. For an analysis of a typical stiffened plate structure, such as a deck of a ship, the use of the Hermitian-beam model (once modified as described above) is recommended due to its attractive cost-effectiveness.

References

[1] ADINA R&D, Watertown. ADINA theory and modeling guide, May 1999.

[2] Bathe K.J. Finite element procedures. Prentice Hall, 1996.

[3] Boot, J.C. and Moore, D.B. Stiffened plates subjected to transverse loading. International Journal of Solids and Structures, Vol. 24, 1: 89-104, 1988.

[4] Cho K.N. and Vorus W.S. An equivalent three-dimensional model for analyzing orthogonal stiffened plate structures. Journal of Ship Research, 31: 101-110, 1987.

[5] Clarkson J. Tests of flat plated grillages under concentrated loads. Trans. INA, 101:129-140, 1959.

[6] Deb A. and Booton M. Finite element models for stiffened plates under transverse loading. Computers and Structures. Vol. 24, 3:361-372, 1988.

[7] Donnel L.H. Beams, plates and shells. McGraw-Hill, 1976.

[8] Gupta A.K. and MA P.S. Error in eccentric beam formulation. International Journal for Numerical Methods in Engineering, 11:1473 – 1483, 1977.

[9] Huber M.T. Die Grundlagen einer rationalen Berechnung der kreuzweise bewehrten Eisenbetonplatten. Zeitschrift des Osterreichischen Ingenieur und Architekten-Vereines, Vol. 66, 30:557-564, 1914.

[10] Hughes O.F. Ship Structural Design. SNAME, 1988.

[11] Kendrick S. The analysis of a flat plated grillage. European Shipbuilding, 5:4-10, 1956.

[12] Miller R.E. Reduction of the error in eccentric beam modeling. International Journal for Numerical Methods in Engineering. 15: 575-582, 1980.

[13] Mukhopadhyay M. and Satsangi S.K. Isoparametric stiffened plate bending element for the analysis of ship's structure. Trans. RINA, 126:141-151, 1984.

[14] O'Leary J.R. and Harari I. Finite element analysis of stiffened plates. Computers and Structures, 21: 973-985, 1985.

[15] Popov E.D. Mechanics of materials. Prentice Hall, 1976

[16] Przemieniecki J.S. Theory of matrix structural analysis, McGraw-Hill, 1968.

[17] Satsangi S.K. A review of static analysis of stiffened plates. Journal of Structural Engineering, vol 15, 4: 117-126.

[18] Timoshenko S.D. and Goodier J.N. Theory of elasticity. McGraw-Hill, 1970

[19] Timoshenko S.D. and Woinowsky-Kreiger S. Theory of plates and shells. McGraw-Hill, 1959.

[20] Troitsky M.S. Stiffened plates. Elsevier, 1976

Appendix A – Incompatibility of complex cross-sections

In general, as the mesh of a given finite element model is refined, the numerical solution of that model converges monotonically to the solution of the mathematical model (see discussion in Chapter 2). This is true provided that the elements used in the model are displacement-based and complete (able to represent rigid body displacement and constant strain states), and the mesh is compatible (i.e. the displacements are continuous across the element assemblage). Under these conditions, as the mesh is refined the numerical solution yields increasingly larger strain energy (but all below the exact strain energy), and hence we approach the solution of the mathematical model from below. In the following we consider a special case in which incompatibility of the displacement field happens to lead to convergence of the numerical solution to the mathematical model solution from above.

In ref. [8] A.K. Gupta examines the influence of the displacement incompatibility in a stiffened plate finite element model, where *Hermitian* plate and beam elements (elements in which the section rotations are obtained by differentiation of the transverse displacements) are used to model the plate and stiffeners, respectively. The incompatibility arises from the fact that the linear longitudinal displacement of the stiffeners is linked to the cubic transverse displacement of the plate, as further discussed below. In the following we briefly describe the error involved with this model, as presented in ref. [8], and then show that the error is eliminated once iso-parametric shell elements are used to model the plate.

The problem can be simplified as a two-dimensional beam with a "T" cross-section, modeled by *two* Hermitian beam elements (one represents the flange and the other represents the web) as described in Figure A-1. This model contains the same displacement incompatibility as the stiffened plate model discussed above, and hence can serve for demonstration. The assembly of the combined stiffness matrix requires the transformation of the stiffness matrix of beam 2 (the web) such that it will

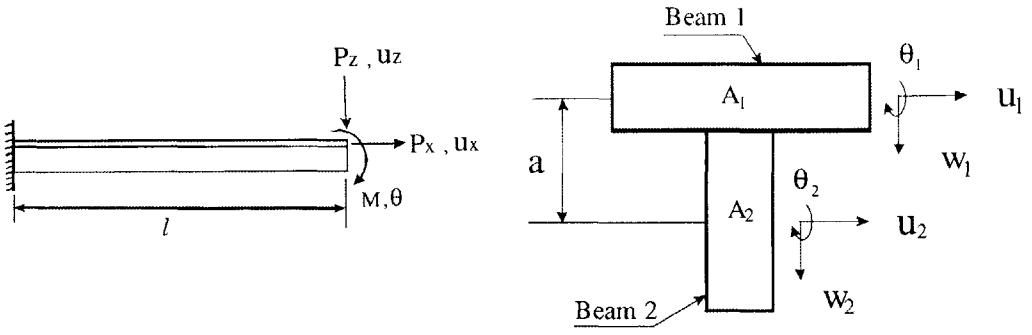

Figure A-1: "T" cross-section modeled by Hermitian beam elements

correspond to the displacements of beam 1 (the flange). Hence, the first step is to determine the transformation matrix. The relation between the displacements of beam 2 and beam 1 is given by

$$\begin{aligned} u_2 &= u_1 - a\theta_1 \\ w_2 &= w_1 \\ \theta_2 &= \theta_1 \end{aligned} \tag{A.1}$$

Accordingly, the transformation matrix, D, takes the form

$$\begin{bmatrix} u_2 \\ w_2 \\ \theta_2 \end{bmatrix} = D \begin{bmatrix} u_1 \\ w_1 \\ \theta_1 \end{bmatrix} \quad ; \quad D = \begin{bmatrix} 1 & 0 & -a \\ 0 & 1 & 0 \\ 0 & 0 & 1 \end{bmatrix} \tag{A.2}$$

The original stiffness matrix of beam 2 (two-dimensional Hermitian beam element without shear deformations) is given by

$$K_2 = E \begin{bmatrix} \frac{A_2}{l} & 0 & 0 \\ 0 & \frac{12I_2}{l^3} & \frac{-6I_2}{l^2} \\ 0 & \frac{-6I_2}{l^2} & \frac{4I_2}{l} \end{bmatrix} \tag{A.3}$$

The transformed stiffness matrix is obtained by

$$K_2^* = D^T K_2 D \tag{A.4}$$

which results in

$$K_2^* = E\begin{bmatrix} \frac{A_2}{l} & 0 & \frac{-A_2 a}{l} \\ 0 & \frac{12I_2}{l^3} & \frac{-6I_2}{l^2} \\ \frac{-A_2 a}{l} & \frac{-6I_2}{l^2} & \frac{A_2 a^2}{l} + \frac{4I_2}{l} \end{bmatrix} \tag{A.5}$$

The total stiffness matrix is obtained by

$$K_{TOT} = K_1 + K_2^* \tag{A.6}$$

which leads to the following displacement-load equation

$$\begin{bmatrix} \frac{A_1 + A_2}{l} & 0 & \frac{-A_2 a}{l} \\ 0 & \frac{12(I_1 + I_2)}{l^3} & \frac{-6(I_1 + I_2)}{l^2} \\ \frac{-A_2 a}{l} & \frac{-6(I_1 + I_2)}{l^2} & \frac{4(I_1 + I_2)}{l} + \frac{A_2 a^2}{l} \end{bmatrix} \begin{bmatrix} u_1 \\ w_1 \\ \theta \end{bmatrix} = \frac{1}{E}\begin{bmatrix} P_X \\ P_Z \\ M \end{bmatrix} \tag{A.7}$$

where P_X, P_Z and M are applied on the centroid of beam 1. Letting $P_X = 0$, w_1 (the tip transverse deflection) is given by

$$w_1 = P_Z \frac{l^3}{3EI^*}(1 + C) + M \frac{l^2}{2EI^*} \tag{A.8}$$

where

$$C = \frac{A_1 A_2 a^2}{4(A_1 + A_2)(I_1 + I_2)} \tag{A.9}$$

and I^* is the moment of inertia of the composite section, given by

$$I^* = I_1 + I_2 + \frac{A_1 A_2 a^2}{A_1 + A_2} \tag{A.10}$$

Considering (A.8), it can be noticed that the well-known expression for the transverse tip deflection of a cantilever beam subjected to moment and transverse load is given here containing the term C, which can be considered as an error term. The error, which leads to a larger tip displacement, is a result of the displacement incompatibility introduced by the beam representing the web. The stiffness matrix presented in (A.3) is based on the assumptions of a linear longitudinal displacement variation, and a cubic variation of the transverse displacement. The latter assumption results in a quadratic variation of the rotation θ_1. Consequently, the variation of the longitudinal displacements at the nodes of beam 2, as given in (A.1), is quadratic, which contradicts the linear variation assumption and hence introduces an incompatibility into the model.

It is interesting to note that an error is introduced to the expression of the vertical tip displacement [as given in (A.8)] only when a transverse force (P_Z) is applied. When only a moment exists, the exact solution by Bernoulli is obtained, since the moment induces a *quadratic* variation of the transverse displacement (w_1) along beam 1. This quadratic variation results into a linear variation of the rotation (θ_1), and hence all the terms in the expression of the longitudinal displacement given in (A.1) are linear. Therefore, the incompatibility discussed above does not take place when only a moment is present.

Once a transverse load is applied, the incompatibility is introduced only in the span *between* the nodes. The geometrical constrains on the degrees of freedom of beam 2 [as

given in (A.1)] result in compatible displacements of beam 1 and beam 2 *at the nodes*, as shown in Figure A-2a. Along the span of the element (i.e. between the nodes) the incompatibility results in overlapping of beam 1 (the flange) and beam 2 (the web), as demonstrated in Figure A-2b. It should be emphasized that when only a moment is applied, the compatibility is maintained along the length of the elements, as well as at the nodes.

Considering now a beam with the same cross-section (as given in Figure A-1), modeled by 2n elements (n in the flange, n in the web) and subjected to a tip load P_Z- as described in Figure A-3. The transverse force and the moment acting on the right hand side of element r (also shown in Figure A-3) are

$$P_{Zr}=P_Z \tag{A.11}$$

$$M_r=P_Z(n-r)l_e \tag{A.12}$$

where l_e is the length of one element. Using (A.8) the tip displacement of one element, treated as cantilever beam, can be given as

$$w_r = P_{Zr}\frac{l_e^{\,3}}{3EI^*}(1+C)+M_r\frac{l_e^{\,2}}{2EI^*} \tag{A.13}$$

Following the same procedure, we can obtain the tip rotation

$$\theta_r = \frac{P_{Zr}l_e^{\,2}}{2EI^*}+\frac{M_r l_e}{EI^*} \tag{A.14}$$

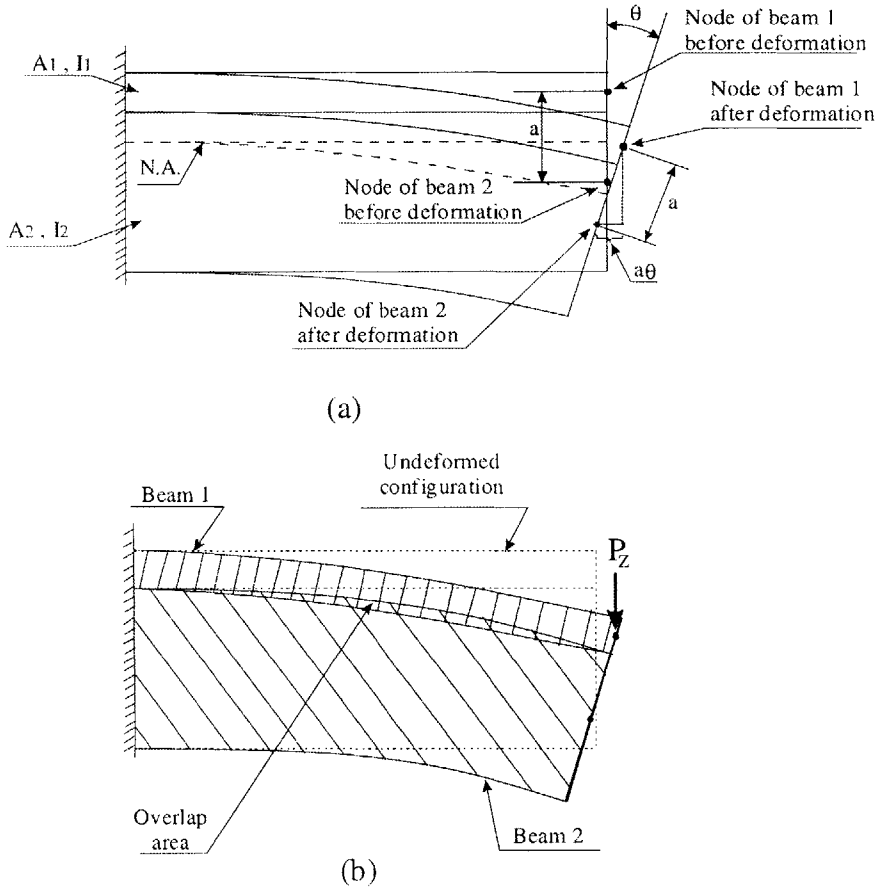

Figure A-2: Geometrical constrains and incompatibility of the displacements of the eccentric beam.

The tip displacement of the beam is accumulated through the elements, and is given by

$$w = \sum_{r=1}^{n} w_r + \sum_{r=1}^{n} \theta_r (n-r) l \tag{A.15}$$

which results in

$$w = \frac{P_Z (n l_e)^3}{3EI^*} \left[1 + \frac{C}{n^2} \right] \tag{A.16}$$

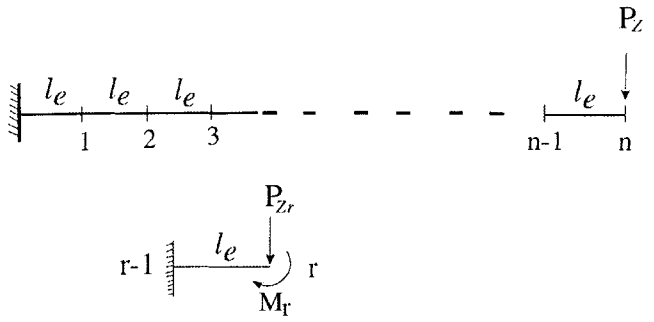

Figure A-3: Cantilever beam modeled with 2n elements – n in the flange, n in the web.

As can be seen, the error term in (A.16) diminishes as n approaches infinity. This means that a refinement of the mesh decreases the error, and hence results in smaller tip deflection. The physical reasoning for the reduction of the error term, as the mesh is refined, is that the gap between the cross-sections of the flange and the web (as shown in Figure A-2b) reduces as the span between the nodes (where the displacements compatibility is maintained) is reduced.

The above analytical result was examined by constructing and solving the corresponding finite element model using ADINA. The "T" cross-section beam (described in Figure 4-1a) was modeled as a combination of two beams (using Hermitian beam elements) – representing the flange and the web. The mesh was refined gradually, and the tip deflection was recorded for each case. The same physical problem was also solved by the classical beam theories by Bernoulli and Timoshenko, and the comparison between the various solutions is given in Figure A-4. As can be seen, the solution of the "all-Hermitian beam element" model converges to the mathematical solution (which is the simple Bernoulli theory when we use Hermitian beam elements without inclusion of shear deformation) from above, as predicted by the analytical result in (A.16). For n=200 the numerical solution for the tip deflection has a 0.165% discrepancy relatively to the Bernoulli solution.

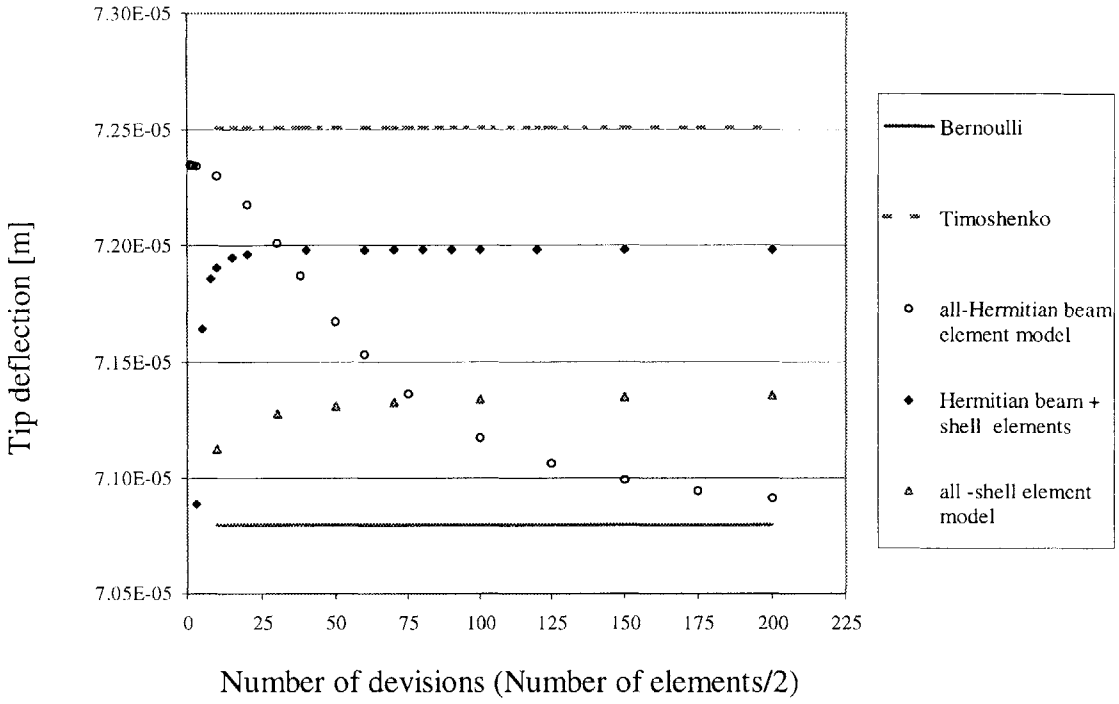

Figure A-4: Comparison of tip deflection solution.

Modeling the same beam with a combination of shell elements (representing the flange) and Hermitian beam elements (representing the web) eliminates the error discussed above, and the finite element numerical solution converges to the mathematical solution from below.

The error is eliminated since the variation of the rotation degrees of freedom of the 4-node isoparametric shell element is *linear* and hence it does not introduce quadratic terms into the longitudinal displacement of the eccentric beam as in the case of modeling the flange by Hermitian beam elements. As discussed above, this trend of convergence is to be expected for a general case of a finite element model solution, as further demonstrated by the solution of the "all-shell" mode